2014

Noncovalent Interactions Involving Microsolvated Networks Of Trimethylamine N-Oxide

Kristina Andrea Cuellar
University of Mississippi

NONCOVALENT INTERACTIONS INVOLVING MICROSOLVATED NETWORKS OF TRIMETHYLAMINE N-OXIDE

Kristina A. Cuellar

A thesis submitted in partial fulfillment
of the requirements for the degree of

Master of Science
Physical Chemistry

University of Mississippi

August 2014

ABSTRACT

This thesis research focuses on the effects of the formation of hydrogen-bonded networks with the important osmolyte trimethylamine N-oxide (TMAO). Vibrational spectroscopy, in this case Raman spectroscopy, is used to interpret the effects of noncovalent interactions by solvation with select hydrogen bond donors such as water, methanol, ethanol and ethylene glycol in the form of slight changes in vibrational frequencies. Spectral shifts in the experimental Raman spectra of interacting molecules are compared to the results of electronic structure calculations on explicit hydrogen bonded molecular clusters. The similarities in the Raman spectra of microsolvated TMAO using a variety of hydrogen bond donors suggest a common structural motif in all of the hydrogen bonded complexes. In particular, the arrangement of hydrogen bonds with TMAO's oxygen atom appears to dictate the extended hydrogen bonded network and is likely the origin of TMAO's osmolytic strength via the indirect effect. Hyperconjugation is observed in both TMAO and the hydrogen bonded solvent molecules. This charge transfer leads to blue shifts in TMAO's C-H stretching modes and a dramatic red shift in methanol's symmetric stretch. The effect is larger in the case of water and is likely the origin of TMAO's blue shifted C-H stretching modes in solution.

ACKNOWLEDGEMENTS

This work has been supported, in part, by the National Science Foundation (EPS-0903787 and CHE-0955550), as well as the University of Mississippi. Much of the computational work was performed in collaboration with the Department of Chemistry at Mississippi College, specifically Dr. David H. Magers and his research group. I would like to thank all of the University of Mississippi's Department of Chemistry and Biochemistry for teaching me much more than just chemistry. The Department of Chemistry at Mississippi State University, specifically the Dr. Keith T. Hollis research group, also merits my gratitude. Most appreciation goes to the Dr. Nathan I. Hammer research group here at Ole Miss, which I have been a part of since my undergraduate career.

TABLE OF CONTENTS

LIST OF FIGURES

CHAPTER 1

NONCOVALENT INTERACTIONS AND THE HYDROPHOBIC EFFECT

1.1 NONCOVALENT INTERACTIONS

There are many types of noncovalent interactions[1] and each of these is fundamentally electrostatic in nature. Noncovalent interactions are different from covalent bonds because they do not involve sharing of electrons. Noncovalent interactions include ionic interactions, van der Waals interactions, hydrophobic interactions and hydrogen bonds, to name a few. Ionic interactions are electrostatic interactions between permanently charged species, or between an ion and a permanent dipole. Van der Waals interactions are weak electrostatic interactions between all atoms, regardless of polarity. They can have attractive/dispersive, and repulsive/steric, components. Hydrophobic interactions are a complex phenomenon associated with ordering of water molecules around nonpolar groups and will be discussed further in Section 1.3.

Hydrogen bonds were first described by Linus Pauling in his 1939 *Nature of the Chemical Bond.* He stated that "Under certain conditions an atom of hydrogen is attracted by rather strong forces to two atoms instead of only one, so that it may be considered to be acting as a bond between them. This is called a *hydrogen bond*…A hydrogen atom with only one stable orbital cannot form more than one pure covalent bond and the attraction of the two atoms observed in hydrogen bond formation must be due largely to ionic forces."[2] Later, the definition of the hydrogen bond changed in the 1960 book *The Hydrogen Bond* by Pimental and McClellan to "A

hydrogen bond exists between the functional group, A-H, and an atom or a group of atoms, B, in the same or different molecules when (a) there is evidence of bond formation (association or chelation), (b) there is evidence that this new bond linking A-H and B specifically involves a hydrogen atom already bonded to A."[3] The importance of hydrogen bonds in biomolecules was described by multiple scientists in the 1950's.[4-5] Hydrogen bonds vary in strength from very strong (15-40 kcal/mol^{-1}), comparable to a covalent bond, to very weak (1-4 kcal/mol^{-1}), comparable to Van Der Waals forces. The nature of hydrogen bonds will be discussed in more detail in Section 1.2.

1.2 HYDROGEN BONDING

The idea of hydrogen bonds has been around for about a hundred years, and the consequences of hydrogen bonding were observed before they were named or described. They have been described by many names such as weak unions, near valence, associations, chelations and more. A simple modern definition of the hydrogen bond is that a strong dipole-dipole or charge-dipole interaction that arises between an acid (proton donor) and a base (proton acceptor). In biological molecules, the hydrogen acceptor is usually an oxygen or a nitrogen and the donor is another electronegative atom. Observing the frequency shifts of the molecular vibrations, especially the X-H bond, has been a useful probe to vibrational spectroscopists in attempts to describe the behavior of hydrogen bonds. Theorists can analyze hydrogen bonds through quantum mechanical interactions such as polarization and charge transfer between molecules, which are both donor-acceptor type interactions. Charge transfer is known as the movement of electrons from the occupied orbitals of one atom to the unoccupied orbitals of another.

The nature of the hydrogen bond depends on the nature of the donor and acceptor groups, and because of this there is a full spectrum of hydrogen bond strengths. Moderate hydrogen bonds are the most common, which are typically 4-15 kcal/mol for bonds with neutral atoms that have unshared lone pair electrons. Even stronger hydrogen bonds in the range of 14-40 kcal/mol form when one atom is charged. Weak hydrogen bonds, less than 4 kcal/mol, generally occur for neutral atoms that are similar in electronegativity.

Water is a molecule with many unique properties. It is composed of four electron pairs and two pairs covalently link hydrogen atoms to a central oxygen atom and the two remaining pairs are nonbonding. The electronegativity of the oxygen atom induces a net dipole moment, and combined with the high dielectric constant of water, which shields oppositely charged ions, it is a good solvent for charged and polar substances. Water can serve as both a hydrogen bond donor and acceptor, with up to four hydrogen bonds per molecule, as shown in Figure 1.1. These properties lead to water having a high boiling point, a high melting point, and a large surface tension.

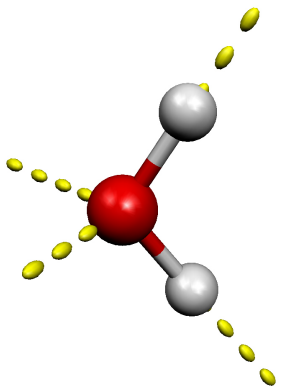

Figure 1.1. Water can serve as both a hydrogen bond donor and acceptor.

1.3 THE HYDROPHOBIC EFFECT

Attempts to elucidate the intriguing behavior of nonpolar solutes in water began in the early 1900's. This behavior is usually termed hydrophobic interactions or effects. In a general sense, the hydrophobic effect has much to do with the reasons why oil and water don't mix. But the basic definition is in which there is a tendency of nonpolar molecules to associate in aqueous solutions. One of the first observations was that of an extremely large negative enthalpy of solvation when nonpolar solutes were introduced to water. It was suggested that water was forming an "ice-like" cage around the solute molecule. It was further realized that aversion of nonpolar solutes in water was also accompanied by a large heat capacity.[6-10] A large heat capacity signifies that the enthalpy and entropy are strong functions of temperature, which means that this aversion can be either driven by entropy or enthalpy.

Mixing polar substances in water is accompanied by an increase in entropy as well as a lower overall energy of the system.[11] The case of nonpolar solutes in water is much different, and the exact mechanism is still unknown.[12-13] The ordering of water near a hydrophobic group leads to an unfavorably large negative change in entropy.[1] There is a slight decrease in enthalpy, but not enough that it can compensate for the large negative entropy. The overall energy of this type of interaction is large and positive which therefore makes this reaction unfavorable.

The Gibbs free energy of a system (ΔG) is the energy associated with a chemical reaction that can be used to do work.[1] The free energy of a system is the sum of its enthalpy (ΔH) plus the product of the temperature and the entropy (ΔS) of the system (Eq. 1.1). The enthalpy is generally thought of as the heat evolved from the system and the entropy a measure of the order or disorder. For a system to proceed spontaneously, the ΔG must be negative. Therefore, having a negative ΔH and a positive ΔS are favorable conditions.

$$\Delta G = \Delta H - T \Delta S \quad (1.1)$$

With this positive free energy in mind when mixing nonpolar solutes in water, it becomes favorable to hide non-polar hydrophobic groups away from the aqueous environment as well as to exclude water molecules. This leads to the typical definition of the hydrophobic effect: it refers to the association or folding of non-polar molecules in an aqueous solution in an attempt to decrease the amount of order the water network must make and therefore increasing the entropy of the system and makes the overall free energy more favorable. It has been suggested that this hydrophobic effect is one of the main factors behind protein folding, protein-protein association, formation of lipid micelles, binding of steroid hormones to their receptors, and many other processes involving amphiphilic molecules and aqueous solutions of nonpolar solutes.[14-15]

Several scientists at the turn of the 20th century noticed that there was a large negative entropy of solvation of simple nonpolar solutes, such as argon or methane, in water.[7,11-15] Scientists were even more surprised when this was compared with the entropy of solvation of ions. One group came up with an idea that was based on a lattice theory of water. They assumed that there are a fixed number of cavities in liquid water and the gas dissolved in water is confined to this fixed number of holes. They concluded that the decrease in entropy was due to the gas molecules being more translationally restricted.[12] Around the same time, Frank and Evans proposed that "when a rare gas atom or nonpolar molecule dissolves in water at room temp, it modifies the water structure in the direction of greater crystallinity."[15] This model has been the most popular idea and was coined the "iceberg" model because it was thought that water was forming an ice-like structure around the solute molecule as the overall structure of water increased. Walter Kauzmann and his group also tried to explain the behavior of nonpolar solutes in water.[14] At his time, it was known that the transfer of nonpolar solute to an aqueous one is exothermic (-ΔH)

which lead him to propose that the system increases in energy solely because of the large negative entropy change. He was also responsible for the first use of the term hydrophobic bond, which he thought was a large driving force for protein folding. A review article by David Chandler in *Nature* tried to explain why hydrophobic interactions were composed of both entropic and enthalpic components.[16] He described the length scale differences of the hydrophobic effect. In the case of a small molecule such as methane, its presence in water requires no breaking of hydrogen bonds. Water molecules can adopt orientations that allow hydrogen bonding to continue uninterrupted around the solute, which is different in the large solute case where solute surface areas larger than one square nanometer make it impossible for adjacent water molecules to maintain a complete hydrogen bonded network. A process that involves significant changes in hydrogen bonding number will have a significant enthalpic component, and a process that requires specific organization of hydrogen bonding will have an important entropic component. As well as a length scale dependence, there is also a temperature dependence, evident from the large change in heat capacity observed. At room temperature for example, the entropic cost in hydrating small hydrophobic species is dominant, but a large enough increase in temperature eventually ends this trend because the importance of maintaining hydrogen bonds no longer exists and the enthalpic part becomes dominant.

Recent research has attempted to describe the hydrophobic effect by means other than free energy changes.[17-19] When discussing hydrophobic interactions, a common and simple method of determining the degree of hydrophobicity or hydrophilicity of a surface is to observe the angle a water droplet makes on that surface. If this contact angle is less than 90°, the surface is deemed hydrophilic, and if the angle is greater than 90° the surface is said to be hydrophobic.[17] Water at a hydrophobic surface can be thought of as similar to water at a liquid vapor interface. Interfacial

tension of pure water is very high compared to alcohols and the addition of a small amount of alcohol decreases the interfacial tension drastically. The decrease in interfacial tension is also seen by a decrease in the contact angle of a water droplet at a hydrophobic surface with the addition of alcohol. The decrease in interfacial tension can be explained by looking at the molecular structure of water and alcohol next to a hydrophobic surface.[17] The hydrophobic surface interferes with the hydrogen bonded network of water so it dislikes being next to the surface and has a high interfacial tension. Addition of alcohol which has both hydrophobic and hydrophilic segments stabilized the structure with the hydrophobic segment of alcohol preferentially going toward the hydrophobic surface and the hydrophilic segment facing away from the surface and towards bulk water.

Rezus and Bakker used femtosecond mid infrared spectroscopy to study the orientational mobility of water molecules in the hydration shells of hydrophobic groups.[18] They used aqueous solutions of hydrophobic solutes with increasing number of hydrophobic segments, specifically, tetramethyl urea, trimethylamine-N-oxide (TMAO), proline and n-methylacetamide. They plotted the mobility of the water as a function of the concentration of solute, and from the slope of their data they calculated that the solvation shell of a TMAO molecule, with 3 hydrophobic methyl groups, contains approximately 12 strongly immobilized O-H groups. They repeated the procedure with the three other solute molecules and the linear relation between the mobility of water and the concentration of solute showed that the immobilized water molecules are part of the hydration shell around the hydrophobic methyl groups of the solutes. The slope of their data gave a value of 3.9 indicating that every methyl group is responsible for the immobilization of approximately four water O-H groups. Further research by Galamba et al. probed the local structure of water in the hydration shells of hydrophobic molecules (xenon, methane, ethane and

benzene) in aqueous solutions simulated with molecular dynamics and compared to neat water at 298 and 283 K.[19] The water at 283 K (10 °C) was used to compare these simulations to that of cold water in attempt to analyze Frank and Evans' iceberg model. The structure in the regions of the first and second solvation shells of these solutions were probed of the oxygen from water radial distribution functions. The radial distribution functions of the solute water mixtures were plotted against the solute to water distance. They plotted the number of water-water donor and acceptor hydrogen bonds for the distinct solvation shells and solutes. The number of hydrogen bonds in the first hydration shell was larger for all solutes, whereas in the second hydration shell, the number of hydrogen bonds is nearly equal to the number in pure water at 298 K. The increase in the number of hydrogen bonds in the first hydration layer is smaller than that observed for neat water at 10 °C but larger than in pure water at room temperature. As well as probing the number of hydrogen bonds, they also wanted to look at the tetrahedrality of water as solute was included. They plotted the probability distributions of the tetrahedral parameter, q, for pure water at 298 and 283 K and for the distinct solutions. Q was determined by the angle made between the oxygen of a water molecule and the oxygen of its nearest neighbors and its value varied from 0, representing an ideal gas, to 1, representing a perfect tetrahedral hydrogen bonded network. A significant enhancement of the tetrahedrality is observed in the first hydration shell relative to neat water at 298 K, and showed that the tetrahedrality of water in the first hydration shell is comparable to that of pure water at 10 °C. These authors moderately support the iceberg model where water molecules near hydrophobic groups adopt more tetrahedral arrangements. They concluded that the enhancement was not larger than that observed for water at 10 °C, which is very different from the iceberg model previously proposed. They believed this ordering should also occur around hydrophobic groups of more complex systems (e.g. amphiphilic molecules and

more complex biological systems). A similar experiment concluded that the amphiphilic molecule TMAO perturbs the water structure in a similar way to that achieved by lowering the temperature of the neat liquid.[20] In other words, spectral data indicated that adding TMAO to water induces the formation of ordered patches of water molecules analogous to the hydrophobic effect.

CHAPTER 2

SPECTROSCOPY

2.1 LIGHT AND MATTER

Spectroscopy refers to the study of the interactions between electromagnetic radiation and matter. Electromagnetic radiation, also known as light, is a continuum of different frequencies of radiation from gamma rays to radio waves (Fig. 2.1). Visible light is a small part of the continuum that is composed of colors from violet to red. Light is composed of both an electric and magnetic field and it possesses both wave and particle behavior. This phenomenon is collectively termed "wave-particle duality." For this reason, waves of light can be thought of as a stream of particles, called photons. The energy of the photons can be calculated with equation 2.1 where E is the energy in joules, h is Planks constant (6.626×10^{-34} Js) and ν is the frequency in Hertz. The frequency, ν, of the wave corresponds to the number of crests that pass a fixed point in a second. The wavelength of the light, λ, is related to the frequency by Equation 2.2, where c is the speed of light (2.997×10^{8} m/s). By mixing these two equations, we can relate the energy of the photon to the frequency of the wave and the speed of light, as shown in Equation 2.3. This equation shows that the frequency of the wave is directly proportional to the energy and the wavelength is inversely proportional to the energy.

$$E = h\nu \tag{2.1}$$

$$c = \lambda\nu \tag{2.2}$$

$$E = \frac{hc}{\lambda} \tag{2.3}$$

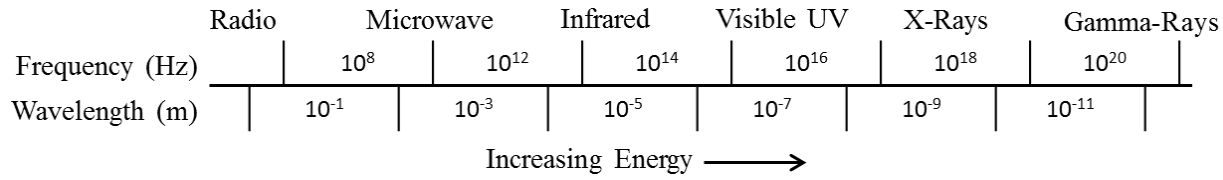

Figure 2.1. Continuum of electromagnetic radiation.

Matter, in the form of molecules can vibrate, rotate, and translate. For example, microwave radiation can be used to study the rotation of molecules and ultraviolet radiation can cause a transition of electrons to higher energy levels. These movements are affected by the interaction of matter with radiation and are called transitions. When light interacts with matter, the light can be absorbed, transmitted, reflected, or scattered (Fig. 2.2). The energies of the transitions are in the order of rotational < vibrational < electronic. As the figure shows, there are many vibrational and rotational states for each electronic state, and it takes more energy to go from one electronic state to another, then it takes more energy to go from one vibrational state to another, and finally it takes the least energy for a molecule to be excited to higher rotational states. This relationship can be seen from the calculation of the energy of the transition shown in Equation 2.4.

$$\Delta E = E_2 - E_1 = h\nu \tag{2.4}$$

Molecules generally exist, at room temperature, in their ground states, which is the lowest energy state. Radiation can cause a transition to a higher energy state called an excited state.

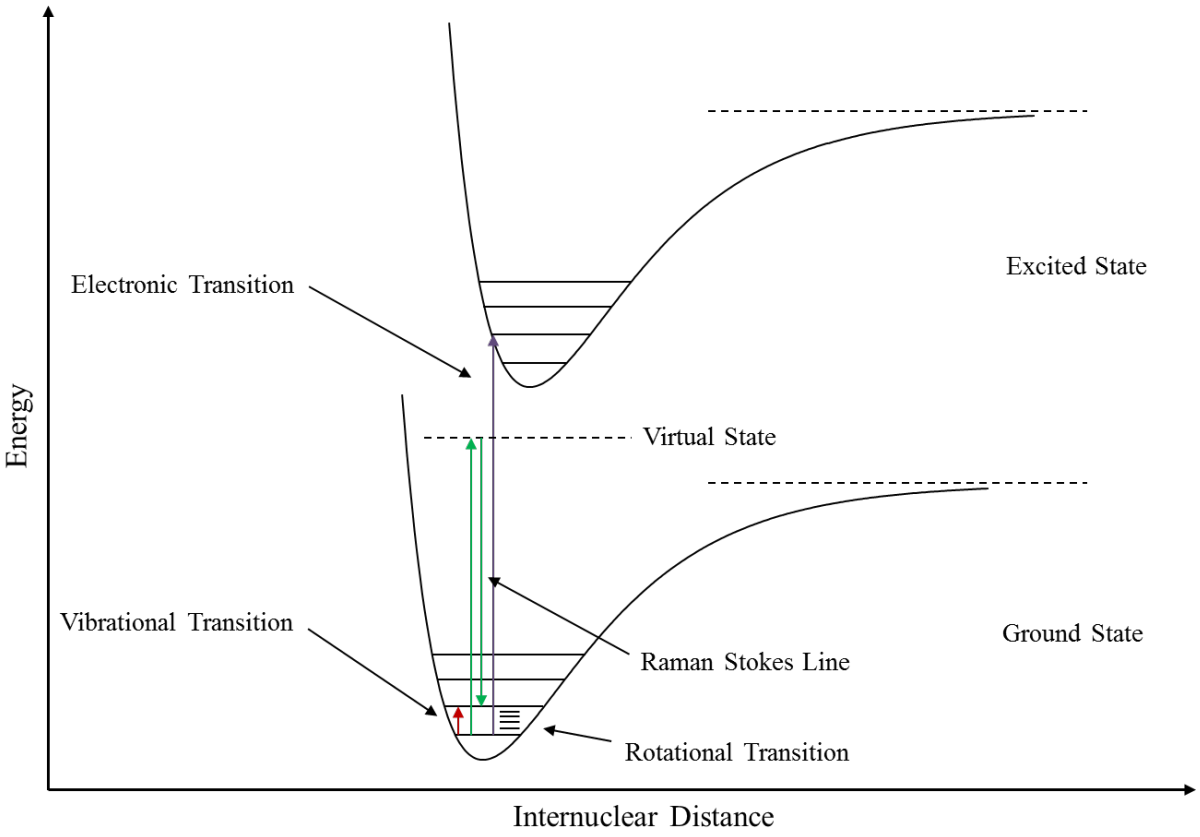

Figure 2.2. Types of electromagnetic transitions.

2.2 VIBRATIONAL SPECTROSCOPY

When thinking about the vibrational motion of molecules, it is common to think of the molecules as balls attached by a spring. The stretching of this spring results in harmonic motion that vibrate following Equation 2.5, where *v* is the frequency of vibration, *f* is the force constant of the spring, and μ is the reduced mass which is calculated by Equation 2.6 with M_1 being the mass of one molecule and M_2 being the mass of the other.

$$v = \frac{1}{2\pi}\sqrt{\frac{f}{\mu}} \tag{2.5}$$

$$\mu = \frac{M_1 M_2}{M_1 + M_2} \tag{2.6}$$

The frequency of vibration can easily be converted to wavenumber values by including the speed of light, c, in centimeters per second to Equation 2.7. The wavenumber (cm^{-1}) is a common unit to describe the frequencies of vibration of molecules. It is in inverse centimeters and corresponds to the number of waves of radiation per centimeter, 1/λ. The vibrational frequencies of molecules are physical properties that are constant for a given molecule. Isotope effects can also be observed with vibrational spectroscopy because the frequency of vibration is related to the mass of the molecules, therefore the spectral peaks shift slightly due to changes in mass.

$$\tilde{\nu} = \frac{1}{2\pi c}\sqrt{\frac{f}{\mu}} \tag{2.7}$$

The position of an atom is determined by coordinates in the x, y, and z directions. This means that each atom has three degrees of freedom so therefore a molecule with N atoms has 3N degrees of freedom of motion. The translational and rotational degrees of freedom are subtracted to give us the internal degrees of freedom of vibration. The translational motion is also made of three coordinates, as is the rotational motion. But for a linear molecule, there will only be two degrees of freedom because rotation about the molecular axis does not displace the nuclei. The

translational and rotational motions do not change the shape of the molecule, but internal degrees of freedom do change the shape but do not move the center of gravity. The number of bands in the vibrational spectrum of molecules is thus equal to 3N-6 for nonlinear molecules and 3N-5 for linear molecules. These are the internal degrees of freedom as well as the number of normal modes of vibration. But because of degeneracy and non-active modes, not all peaks may be experimentally observed. Another possibility is that there may be more peaks predicted and these can arise because of overtones and combination bands which are dependent on the anharmonicity of the vibration. Anharmonicity arises when the restoring forces are not linearly proportional to the nuclear displacement coordinates. Infrared spectroscopy can be used in conjunction to Raman spectroscopy because they both measure the vibrational frequencies of molecules upon irradiation, but in general, a peak that is IR active is not necessarily Raman active. There are many ways a molecule can vibrate and most are classified as either bending or stretching modes. Stretching is when the bond lengths of the molecule change and bending is when the bond angles change. There are symmetric and asymmetric stretching modes and in plane and out of plane bending motions. When a molecule transitions from the ground state to the first vibrational state, this gives rise to the fundamental transition band, and this is the most likely type of transition to occur. If the molecule is excited to a higher vibrational level, it is said to be an overtone. For example, when the molecule is excited to the second vibrational energy level, this band is called the first overtone band. These overtones arise at frequencies that are approximately integer multiples of the fundamental band, and they are usually very weak bands compared to the fundamental. Combination and difference bands arise from mixing of vibrational modes, either at the frequency of the sum of the two bands or the difference of the two bands.

2.3 RAMAN SPECTROSCOPY

The consequences of scattered radiation were first observed by Sir C. V. Raman in 1928, and were therefore named after him. The frequency shifts of scattered radiation are a direct measurement of the vibrational frequencies of a molecule. Raman spectroscopy is usually thought of as a compliment to infrared spectroscopy because the selection rules of the two are different. Infrared spectroscopy depends on the change in dipole moment of the molecule whereas Raman spectroscopy depends on the molecular polarizability or induced dipole moment. Polarizability can be visualized as a distortion of the electron cloud. The induced dipole moment, μ_{ind}, of a molecule comes from the polarizability, α, multiplied by the electric field, E (Eq. 2.8).

$$\mu_{ind} = \alpha E \tag{2.8}$$

The electric field oscillates with the same incident frequency of light, v_0 (Eq. 2.9), and emits radiation of this frequency in all directions. This is elastic scattering.

$$E = E_0 \cos 2\pi v_0 t \tag{2.9}$$

The polarizability can be described with a power series relative to the vibrational coordinate, Q, that oscillates at the vibrational frequency, v_i, where A is the amplitude of the vibration (Eqs. 2.10 and 2.11).The zero subscript indicates the value of the energy and polarizability at equilibrium position.

$$\alpha = \alpha_0 + \left(\frac{d\alpha}{dQ}\right)_0 Q \tag{2.10}$$

$$Q = A \cos 2\pi v_i t \tag{2.11}$$

By substituting and combining the above equations, it can be shown that the induced dipole moment is made up of three parts with the terms corresponding to elastic Rayleigh scattering, inelastic anti-Stokes scattering and inelastic Stokes scattering respectively (Eq. 2.12 and Fig. 2.3).

$$\mu_{ind} = \alpha_0 E_0 \cos 2\pi v_0 t + \frac{1}{2}\left(\frac{d\alpha}{dQ}\right)_0 AE_0[\cos 2\pi(v_0 + v_i)t + \cos 2\pi(v_0 - v_i)t] \quad (2.12)$$

For a molecule to display Raman activity, the transition dipole integral must be nonzero, meaning there is a change in polarizability (Eq. 2.13), where P represents the transition moment. The wavefunctions, Ψ, correspond to the ground state and the first excited vibrational states respectively, quantum numbers $v = 0$ and $v = 1$.

$$P = \int \Psi_1 \mu_{ind} \Psi_0 dQ = E \int \Psi_1 \alpha \Psi_0 dQ \neq 0 \quad (2.13)$$

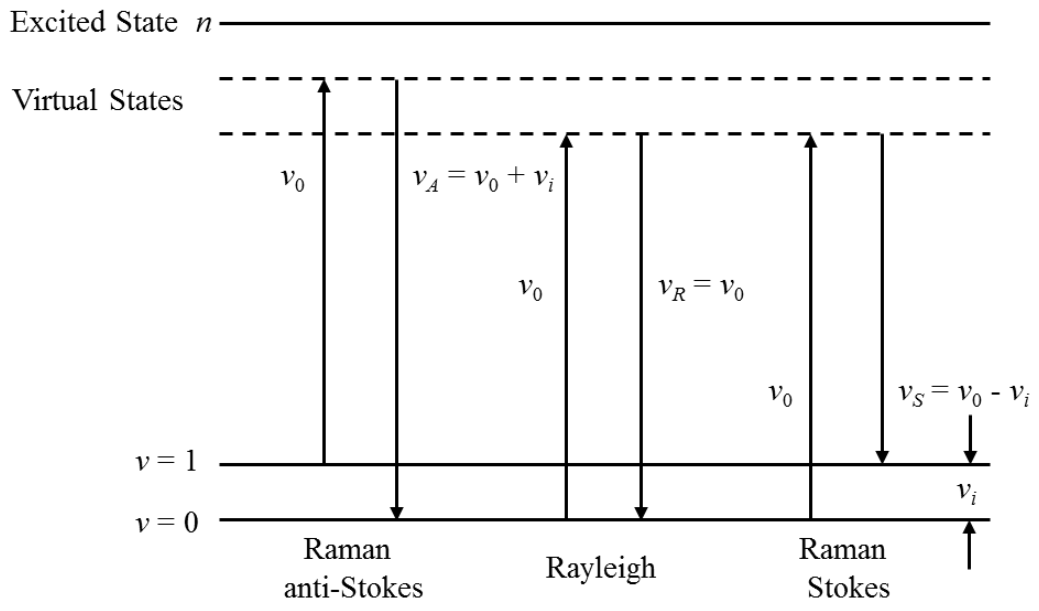

Figure 2.3. Raman scattering.

When radiation is imposed on a molecule, the molecule can either absorb, emit or scatter the light. Raman spectroscopy measures the scattered radiation. There are three types of scattering: Rayleigh scattering, Stokes scattering and anti-Stokes scattering (Fig. 2.3). The most common type is Rayleigh scattering and it occurs when the scattered radiation has the same frequency as the source radiation, also called elastic scattering. Stokes and anti-Stokes are examples of inelastic scattering, where the frequency of the scattered radiation is lower or higher than the

source radiation respectively. The spectral lines that result from inelastic scattering are called Raman lines, and only about 1 in a million photons are scattered this way. The energy difference between the scattered and source light correspond to vibrational transitions of the molecule. When the source photon collides with the molecule, the molecule increases in energy to a virtual state which is between the ground state and first excited electronic state. If the molecule vibrates with more energy after collision with the source photons, the scattered photon decreases in energy equal to the vibrational energy gained by the molecule, Stokes scattering. This is Raman scattering, and the energy of the scattered photon corresponds to the source energy minus the change in energy from the ground and first excited vibrational states. The energy difference between the ground and first excited states corresponds to the IR vibrational frequencies, and if the line is IR active a peak would occur at this frequency. For this reason, Raman spectra are usually plotted with these Raman frequency shifts in wavenumbers in order to directly compare to IR spectra. Anti-Stokes scattering is less common than Stokes, and results from a decrease in energy upon interaction with the source radiation.

2.4 EXPERIMENTAL METHODS

To perform Raman spectroscopy, a light source, typically a laser, is used to excite the molecules of study. The 514.5 nm line from an argon ion laser was employed in this research. Because Raman spectroscopy measures the scattering of the photons, a detector is placed perpendicular to the light source. A monochromatic light source is required and the signal is directly related to the intensity of the source. This is why lasers have become the most popular light sources for Raman spectroscopy, they are intense and monochromatic. Because the intensity of the measured scattering is proportional to the excitation frequency, shorter

wavelength sources produce more scattered light, but with a disadvantage being that higher energy light can cause the molecules to degrade or fluoresce.

A photomultiplier tube (PMT) is a traditional type of detector. Because Raman scattering only occurs in about 1 in a million photons, the photomultiplier tube is needed to amplify the signal. The PMT must be operated at cold temperatures in order to avoid dark current which is caused by stray electrons in the PMT. There are two phases to the cooling: one cooler cools water down to 10 °C and sends this to the thermoelectrically cooled detector which then cools the Ramanor HG2-S PMT detector to -30 °C.

The double grating scanning spectrometer employed here is capable of scanning at any speed the experimenter desires. For example a fast scan (5-10 cm^{-1}/s) can be used to quickly scan a region to determine if any vibrational structure is present. For optimum accuracy, slower scan speeds are preferable and can go down to just above 0 cm^{-1}/s. A scan speed of 2 cm^{-1}/s was typically employed for this research.

A custom vacuum apparatus was constructed for analysis of solid phase samples during microsolvation by the solvent vapor of choice (Figs. 2.4 and 2.5). The apparatus consists of a solid sample chamber connected to a vacuum gauge with an input tube as well as a vacuum or output tube connected to a rotary vacuum pump. The top of the sample chamber is sealed with a quartz window. The input tube of the vacuum chamber connects to a second chamber which houses the solvent of choice. Both the input and output tubes are connected to valves which allow the control of gas flow in or out of the solid sample chamber.

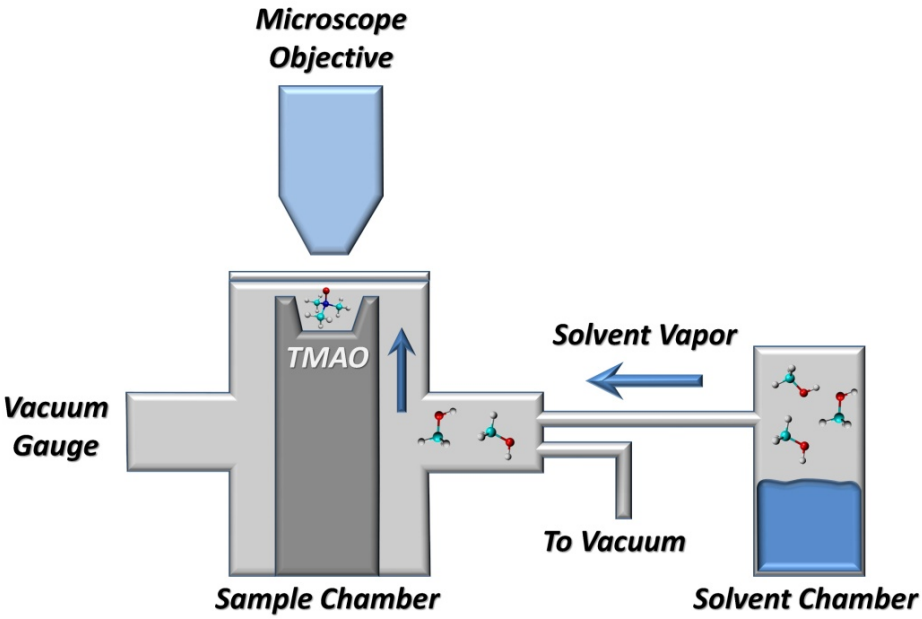

Figure 2.4. Schematic of a microsolvation apparatus.

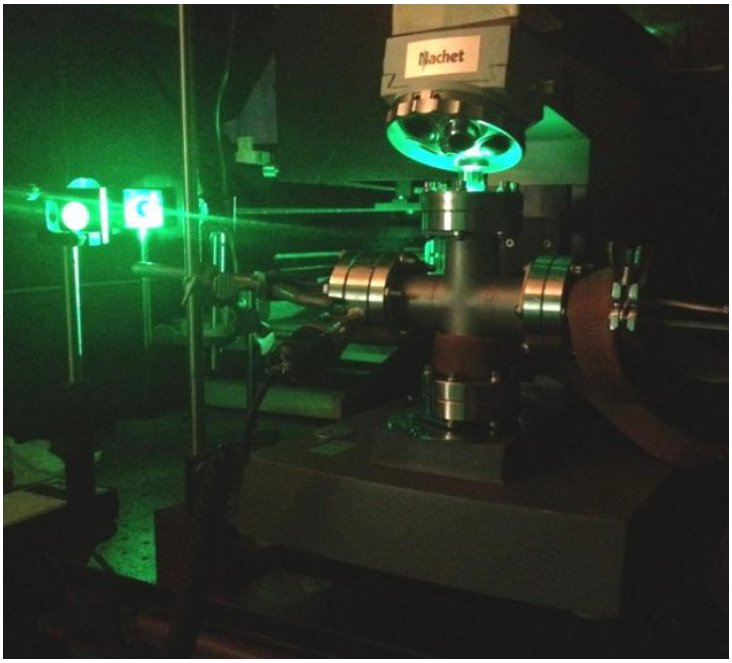

Figure 2.5. Photograph of the apparatus while in use.

CHAPTER 3

COMPUTATIONAL CHEMISTRY

3.1 COMPUTATIONAL BACKGROUND

Quantum mechanics is the study of matter and energy which display wave and particle-like properties, and therefore cannot be accurately described with classical mechanics. Quantum mechanics largely revolves around solving the Schrödinger equation (Eq. 3.1).

$$\hat{H}\Psi = E\Psi \tag{3.1}$$

$\hat{H}$, the Hamiltonian, corresponds to the total energy operator for the time-independent wave function, Ψ, and E is the total energy of the system. The Hamiltonian takes into account the nuclei kinetic energy ($\hat{T}_n$), the electron kinetic energy ($\hat{T}_e$), nuclear-nuclear repulsion ($\hat{V}_{nn}$), nuclear-electron attraction ($\hat{V}_{ne}$), and electron-electron repulsion ($\hat{V}_{ee}$) (Eq. 3.2).

$$\hat{H} = \hat{T}_n + \hat{T}_e + \hat{V}_{nn} + \hat{V}_{ne} + \hat{V}_{ee} \tag{3.2}$$

For large systems, the Schrödinger equation becomes very difficult to solve, so approximation methods such as the Born-Oppenheimer approximation are used. This approximation method separates the electronic and nuclear portions of the Schrödinger equation so that the electronic portion can be solved. Unfortunately, the time-independent Schrödinger can only be solved exactly for one electron systems, (e.g. the hydrogen atom) so more approximations must be made for systems with more than one electron.

To solve the Schrödinger equation for many-electron atoms, a simple starting point is to use the Hartree-Fock Self-Consistent Field (HF-SCF) method which expresses the wavefunction as a Slater determinant with entries corresponding to modified hydrogen atom orbitals (Eq. 3.3).[21] This method solves the many-electron problem by computing the product of multiple one electron wavefunctions. This method looks to find the lowest energy of the ground state atom without respect to electron-electron correlation. By using a Slater determinant, the Pauli exclusion principle is taken into account as well as the asymmetry of the wavefunction. The Pauli exclusion principle states that no two electrons can occupy the same spin orbital, and the antisymmetry means that the wavefunction changes sign when electrons change spatial and spin coordinates. Spin orbitals are represented by χ_i (i = 1, 2, ..., n) and electrons by x_n (n = 1, 2, ..., n), with n being equal to the number of electrons in the system. The Pauli exclusion and asymmetry issues are fixed because when two electrons change spin, the determinant changes sign, but when two electrons are of the same spin, the determinant equals zero.

$$\Psi_{HF} = \frac{1}{\sqrt{n!}} \begin{bmatrix} \chi_1(x_1) & \chi_2(x_1) & \cdots & \chi_n(x_1) \\ \chi_1(x_2) & \chi_2(x_2) & \cdots & \chi_n(x_2) \\ \vdots & \vdots & \cdot & \vdots \\ \chi_1(x_n) & \chi_2(x_n) & \cdots & \chi_n(x_n) \end{bmatrix} \tag{3.3}$$

Because the HF-SCF method does not take into account electron-electron correlation, the angular part of the wavefunction is equivalent to the one electron hydrogen atom. To solve this problem basis functions are used to solve the radial part of the wavefunction based on the variational method. A trial wavefunction is used and the variation theorem states that the calculated energy is always higher than or equal to the true energy of the system (Eq. 3.4).[21] Trial wavefunctions are continually tested to find the lowest possible energy, which gets closer to the true value.

$$E_{HF} = \langle \Psi_{HF} | \hat{H} | \Psi_{HF} \rangle \geq E_{True} \tag{3.4}$$

Basis sets are a combination of functions which are used to describe molecular orbitals. The more basis functions, the more accurate the calculation will be. At least one basis function, ζ, must be used to describe the molecular orbitals. Basis functions, □$_i$, as well as an expansion coefficient, C_i, make up the wavefunction, where N is the number of basis functions. Here double ζ, DZ, and triple ζ, TZ, augmented correlation consistent basis sets have been applied. It is necessary to use augmented, or diffuse, functions when studying long-range noncovalent interactions.

$$\Psi = \sum_i^N C_i \phi_i \tag{3.5}$$

Post Hartree-Fock methods, have been used to account for electron-electron correlation. With M□ller-Plesset (MP) perturbation theory, the Hartree-Fock Hamiltonian is slightly perturbed.

$$\hat{\mathrm{H}}|\Psi_n\rangle = (\hat{\mathrm{H}}_0 + \hat{\mathrm{V}})|\Psi_n\rangle \tag{3.6}$$

$\hat{\mathrm{V}}$ corresponds to the perturbation and the perturbation is equal to the difference of the two Hamiltonians. A pertubative parameter, λ, is added to allow for a power series expansion.

$$(\hat{\mathrm{H}}_0 + \lambda\hat{\mathrm{V}})|\Psi_n\rangle = \mathrm{E}_n|\Psi_n\rangle \tag{3.7}$$

$$E_n = E_n^{(0)} + \lambda E_n^{(1)} + \lambda^2 E_n^{(2)} + \cdots \tag{3.8}$$

$$|\Psi_n\rangle = |\Psi_n^{(0)}\rangle + \lambda\,|\Psi_n^{(1)}\rangle + \lambda^2\,|\Psi_n^{(2)}\rangle + \cdots \tag{3.9}$$

The wavefunction and energy equations are expanded as shown above and then substituted back into the Schrödinger equation.

$$\hat{\mathrm{H}}_0\,|\Psi_n^{(0)}\rangle + \lambda\big[\hat{V}|\Psi_n^{(0)}\rangle + \hat{\mathrm{H}}_0|\Psi_n^{(1)}\rangle\big] + \lambda^2[\hat{\mathrm{H}}_0|\Psi_n^{(2)}\rangle + \hat{V}|\Psi_n^{(1)}\rangle] + \cdots =$$

$$E_n^{(0)}\Psi_n^{(0)} + \lambda[E_n^{(1)}\Psi_n^{(0)} + E_n^{(0)}\Psi_n^{(1)}] + \lambda^2[E_n^{(2)}\Psi_n^{(0)} + E_n^{(1)}\Psi_n^{(1)} + E_n^{(0)}\Psi_n^{(2)}] + \cdots \tag{3.10}$$

This equation can be partitioned down to n^{th} order approximations by combining λ^n terms.

$$E_n^{(0)} = \langle \Psi_n^{(0)} | \hat{H}_0 | \Psi_n^{(0)} \rangle \quad (3.11.a)$$

$$E_n^{(1)} = \langle \Psi_n^{(0)} | \hat{V} | \Psi_n^{(0)} \rangle \quad (3.11.b)$$

$$E_n^{(2)} = \langle \Psi_n^{(0)} | \hat{V} | \Psi_n^{(1)} \rangle \quad (3.11.c)$$

These equations correspond to n^{th} order corrections, such that the first Eq. 3.11.a corresponds to the zero order MP correction, Eq. 3.11.b is the first order MP correction, MP1, and Eq. 3.11.c is the second order MP correction, MP2. The zeroth order MP correction plus the first order MP correction is equivalent to the Hartree-Fock approximation, and the first MP correction which takes into account electron-electron correlation is the MP2 approximation.

As well as ab initio methods such as the MP method, density functional theory (DFT) methods can also be utilized to describe a molecular system. DFT is different from ab initio methods in that it does not seek to find an approximation to the wavefunction. DFT methods simply calculate the electron probability density. DFT methods are based on Hohenberg-Kohn theorems. The first theorem states that all electronic properties can be determined by ground state electron probability densities. The second theorem states that the calculated electron density will always be greater than the true ground state energy. The wavefunction only requires four variables per electron: 1 spin and 3 spatial (*x,y,z*). Here, the B3LYP hybrid functional comprising Becke's three parameter functional[22] using the LYP correlation functional of Lee, Yang, and Parr[23] has been utilized.

Natural bond orbital (NBO) calculations are used to determine electron density of atoms as well as the bonds between atoms. NBO calculations can provide a very accurate molecular structure, and the maximum electron density of bonds is ideally near two electrons. The valence bonding orbitals of the atoms are paired to valence antibonding orbitals, and usually if the

bonding orbital is near two electrons, the corresponding antibonding orbital has an electron occupation near zero. In the case of noncovalent interactions, the filled orbitals from the donor atom transfer some charge to the unfilled orbitals of the acceptor atom, donor-acceptor interactions.[24] Hyperconjugative effects are indicated when the valence bonding orbitals are lower in charge and the antibonding orbitals are higher in charge relative to the non-interacting atoms. In other words, the charge is transferred from bonding to antibonding orbitals when electrons can be delocalized.

3.2 COMPUTATIONAL METHODS

Optimum equilibrium geometries and corresponding electronic energies were determined using density functional theory.[25-26] The B3LYP hybrid functional with the augmented correlation consistent basis set aug-cc-pVTZ by Dunning and co-workers was utilized.[27-28] The vibrational frequencies were also calculated anharmonically with the MP2 method and the aug-cc-pVTZ and aug-cc-pVDZ basis sets to aid in the assignment of fundamentals and combination bands. Natural bond orbital (NBO) calculations were performed using the B3LYP method and aug-cc-pVTZ basis set to determine the influence of charge transfer on the experimentally observed molecular interactions.

For the TMAO project presented in Chapter 4, we collaborated with Prof. David Magers (Mississippi College) for some of the computational work. Prof. Magers optimized the geometries of molecular clusters and performed anharmonic frequency calculations. As a part of this thesis, geometry optimizations, NBO calculations, anharmonic calculations, and simulations of Raman spectra were performed at the University of Mississippi.

CHAPTER 4

NONCOVALENT INTERACTIONS IN MICROSOLVATED NETWORKS OF TRIMETHYLAMINE N-OXIDE

4.1 ABSTRACT

The effects of the formation of hydrogen-bonded networks on the important osmolyte trimethylamine N-oxide (TMAO) are explored in a joint Raman spectroscopic and electronic structure theory study. Spectral shifts in the experimental Raman spectra of TMAO and deuterated TMAO microsolvated with water, methanol, ethanol, and ethylene glycol are compared to the results of electronic structure calculations on explicit hydrogen bonded molecular clusters. Very good agreement between experiment and theory suggests that it is the local hydrogen-bonded geometry at TMAO's oxygen atom that dominates the structure of the extended hydrogen bonded networks and that TMAO's unique stabilizing abilities are a result of the "indirect effect" model. Natural bonding orbital (NBO) calculations further reveal that hyperconjugation results in vibrational blue shifts in TMAO's C-H stretching region when solvated and a dramatic red shift in methanol's C-H stretching region when hydrogen bonding with TMAO.

4.2 INTRODUCTION

Trimethylamine N-oxide (TMAO) belongs to a class of small biomolecules called osmolytes, which are essential in the biological regulation of water. Some osmolytes, such as urea, are responsible for the denaturing of proteins whereas TMAO is extremely effective in counteracting this denaturation.[29-30] Despite the importance of TMAO's biological activity, the exact mechanism behind TMAO's stabilizing abilities has to date not been fully elucidated. In fact, there persists a controversy as to the molecular origin of the mechanism being a "direct effect" or "indirect effect".[31-33] A direct effect is one in which the osmolyte directly alters the structure of the protein backbone, whereas an indirect effect is one in which the structure of the solvent is changed by the osmolyte which in turn changes the structure of the protein.[29,34] Interrogating the effects of noncovalent interactions between osmolytes and their solvents are therefore crucial for understanding and elucidating the mechanism of protection of TMAO.

The large dipole moment of TMAO has been suggested as an important contributing factor in its ability to stabilize biologically relevant aqueous systems.[35-43] The structure of neighboring water molecules are expected to be affected by such a large dipole moment, supporting the indirect effect mechanism.[36] Researchers have also recently suggested that the main factor behind TMAO's protective behavior is a slowdown of the solvent rotational dynamics.[44-45] Another possible factor leading to the stabilization effect of TMAO may be due to the nature of the N-O bond, which is unique because it can serve as a nucleophile or an oxidant.[46]

It is well accepted in the literature that TMAO strengthens hydrogen bonds in aqueous solutions and also encourages the creation of more water-water hydrogen bonds with greater spatial ordering.[47] Water also takes on a characteristic ice-like structure when in the vicinity of molecules such as TMAO that possess both hydrophobic and hydrophilic groups.[48] The water

molecules preferentially hydrogen bond to the hydrophilic group, which in turn decreases the mobility of the water molecules and leaves a void near the hydrophobic group. The water molecules that are surrounding this void space become essentially immobilized and "ice-like," and do not directly interact with the hydrated molecule.[15,18] This collective phenomenon is commonly referred to as the hydrophobic effect.[48]

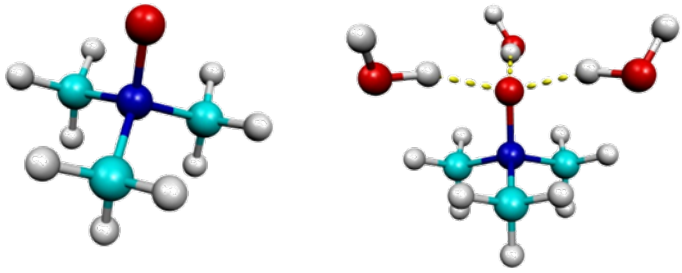

Figure 4.1. Optimized molecular structure of TMAO (left) as well as TMAO with three water molecules attached (right).[49]

We recently elucidated the explicit effects that hydrogen bonded networks of water have on TMAO and showed through good agreement between experiment and theory that each TMAO molecule hydrogen bonds, on average, to three water molecules.[49] Figure 4.1 shows the structure of TMAO and also the molecular cluster geometry that agreed best with the experimental Raman spectra of aqueous TMAO solutions. We also showed that the water network does not directly interact with the methyl groups to a substantial degree and the best agreement with experiment stemmed from theoretical structures including such a void space.[47] Our previous work suggested that the hydrophobic effect plays a significant role in TMAO's ability to order hydrogen bonded water networks. In that study, we not only studied aqueous solutions of TMAO but also monitored time-resolved microRaman spectra at the point of microhydration of TMAO in a humid atmosphere. Such measurements at the solid/vapor interface allow for a better description

of the intimate intermolecular interactions taking place than can be accomplished by examining bulk solutions of different concentrations. Other recent spectroscopic studies have also shown that water molecules on a hydrophobic surface interact differently - as a separation medium - than when in solution.[50-53]

Our previous study only investigated the special case of TMAO interacting with water. Here, we focus on the effects that noncovalent interactions have on TMAO by molecules which cannot form as extensive hydrogen bonded networks. Such molecules include methanol, ethanol, and ethylene glycol. Both methanol and ethanol are amphoteric and amphiphilic molecules, which contain a hydrophobic group of some hydrocarbon (e.g. CH_3 and CH_2CH_3) as well as a hydrophilic O-H group. Using a custom vacuum chamber, we record the vibrational spectra of TMAO as microsolvation layers are gradually deposited onto TMAO. By tracking the Raman spectra of TMAO from the first step of solvation to fully solvated TMAO, we are able to directly compare the effects of noncovalent interactions with the different solvent molecules.

In addition to interrogating the effects of noncovalent interactions on TMAO, we also explore the effect that TMAO exerts on the solvent molecules. Many previous spectroscopic studies have analyzed the effects of noncovalent interactions on methanol's and ethanol's C-O[54-56], C-H[55,57-61], and O-H[54-55] stretching vibrations. For example, Sun et al. demonstrated that ethanol and water vapor behave very differently when interacting with a surface.[62] Whereas ethanol forms a monolayer, water forms a multilayer on the surface due to the fact that water can continually function as a hydrogen bond donor/acceptor and create an extended hydrogen bonded network, while ethanol cannot.[62] Interactions between TMAO and alcohols are of interest because the organic component limits the possibility of hydrogen bond network growth and because it was recently demonstrated that the rotational dynamics of alcohols are slower than

that of water, due to the lack of the ability to form extended hydrogen bonded networks.[63] As well as the decreased ability to form hydrogen bonded networks, alcohols also form weaker hydrogen bonds than water.[64] The hydrogen bonds in ethanol also present a higher degree of thermal stability than those with methanol due to the longer alkyl chain.[65] Venkatesu et al. recently studied the interactions between TMAO and the amphiphilic polymer poly(N-isopropylamide) (PNIPAM) in aqueous solution in an attempt to gain insight into the molecular mechanism between protein and TMAO.[66] These authors showed that TMAO weakens hydrogen bonds between the polymer and water, which in turn procures the collapse of the hydrophobic character of the macromolecule.

It has previously been reported both experimentally and theoretically that the O-H group of water and alcohols exhibit a red shift (shift to lower frequency) in solution, depending on the concentration of solute.[20,67-70] Raman spectroscopy was utilized by Onori and Santucci to examine the hydrophobic behavior of TMAO in aqueous solutions.[20] The O-H stretching region (2800-3800 cm^{-1}) of water and the C-H stretching band (2900-3100 cm^{-1}) of TMAO were examined in an attempt to explain the molecular mechanism of protein stabilization/denaturation counteraction by TMAO. The authors noted a small red shift in the O-H stretching region of water and did not see any variations in the C-H stretching region of TMAO. This was the first use of Raman spectroscopy to examine the noncovalent interactions between TMAO and water, which demonstrated that the hydrogen bonds created in solution are stronger than in the pure solvent itself. In addition, Raman spectra of TMAO have been reported when interacting with various solvents.[71-74] For example, Goubeau and Fromme previously measured the Raman spectra of TMAO in methanol solutions and assigned spectral features to normal modes.[73]

Vibrational normal modes of alcohols that are most usually influenced by hydrogen bonding are the O-H stretching and bending modes, as well as C-O stretching modes.[75-78] Shifts in vibrational frequencies are helpful in determining the hydrogen bonding behavior of amphoteric molecules, with red shifts occurring when an alcohol is acting as a proton donor and blue shifts when acting as a proton acceptor when properly hydrogen bonded.[79] A proper hydrogen bond is one in which the hydroxyl group of an alcohol acts as a hydrogen bond donor, and an improper hydrogen bond is one in which the hydrogen atoms of the organic unit act as the hydrogen bond donor, and the same applies to hydrogen bond acceptors. For example, in 2009 Keefe et al. performed a Raman and FTIR spectroscopic study and showed that the C-H stretching region of methanol exhibits a blue shift with decreasing methanol mole fraction when interacting with either acetonitrile or water in binary mixtures, indicating that improper hydrogen bonding is plausible.[80] Later, Keefe and Istvankova studied changes in vibrational frequencies of the O-H, C-H and C-O vibrations of methanol involved in proper and improper hydrogen bonds.[81] They concluded that when methanol is acting as hydrogen bond donor, the O-H and C-H bands are red shifted if properly hydrogen bonded and the C-H region blue shifts if improperly hydrogen bonded. If methanol is acting as a hydrogen bond acceptor, a blue shift is observed whether it be proper or improper hydrogen bonding. Similarly, blue shifting of ethylene glycol/water mixtures have been recorded in solutions of high water concentration and low ethylene glycol concentration demonstrating that in this case ethylene glycol acts as an efficient hydrogen bond acceptor.[82] There have been many studies in agreement with red shifted C-H and O-H vibrational modes,[20,67-70,83-84] and also some have demonstrated the opposing blue shifted modes.[83,85-86]

In methanol/water mixtures with low methanol content, it has been shown that the Raman peaks of methanol do not shift appreciably, indicating that the methanol molecules are contained

in a solvation shell of water and that the methanol molecules are not considerably interacting with each other.[55] In methanol/water mixtures with higher methanol content, however, the methanol molecules are forced to interact and their O-H groups are pushed farther apart. The O-H band in such methanol/water mixtures red-shift compared to pure liquid methanol, suggesting that the bond is being weakened. In pure liquid methanol, it has been suggested that methanol clusters composed of trimers, tetramers, and pentamers dominate the local structure.[87] Adding other hydrogen bond donors competes with these networks. The frequencies of the C-H vibrational stretches of methanol increase with the addition of water or other polar groups and decrease with the addition of less polar groups.[59-61] In the case of ethanol, the concentration of ethanol in an aqueous solution can even be determined by analyzing the Raman vibrational frequency shifts in the methyl stretching region.[88]

When water molecules hydrogen bond to the hydroxyl group of the alcohol and the structure of bulk water is conserved, this has been referred to as "incomplete mixing" at the molecular level.[89] This hydrophobic segregation suggests that at low methanol concentrations in aqueous solution, the methanol molecules orient their methyl groups away from the water layer and this is concluded by the loss in entropy of the solution as opposed to the increase in entropy which occurs with ideal solutions.[90] In fact, the hydrophilic and hydrophobic forces of alcohols play a large role in its solvation structure and dynamics.[91] In our earlier study, however, we showed that microhydration of TMAO resulted in the most dramatic changes in its Raman spectra and that there are no further spectroscopic effects with bulk dilution once TMAO is initially solvated.[49] This result suggests that the oxygen atom on TMAO may dominate the extended hydrogen bonded network.

Walker et al. recently demonstrated that methanol and ethanol behave differently at a solid/liquid interface than in the liquid or gaseous phases. Due to their size, ethanol molecules have a more difficult time adsorbing to every available site on a solid/liquid interface because they occupy approximately twice the area of a methanol molecule.[92] In the liquid state, methanol participates in approximately 1.9 hydrogen bonds per molecule[93] and can participate in a total of three hydrogen bonds, while surface bound methanol can only participate in a total of two.[94] It has also been shown that alcohols with less than six carbons orient their methyl groups away from an interface.[95]

Spectral shifts in the Raman vibrational spectra of TMAO when microsolvated with water, methanol, ethanol, and ethylene glycol allow us here to explore the effects that different hydrogen bonded networks have on TMAO. By obtaining time-resolved Raman spectra of TMAO in the presence of these vapor phase hydrogen bond donors, we are able to observe the effects of gradual microsolvation by these molecules on TMAO.[94] Comparison of the experimental shifts in the Raman spectra of TMAO[42,72,96-98] when microsolvated to theoretical predictions allows for a molecular-level description of these hydrogen bonded interactions.

4.3 EXPERIMENTAL SECTION

Spectroscopic Methods. Commercial grade anhydrous trimethylamine N-oxide (Sigma-Aldrich), D9-trimethylamine N-oxide (Cambridge Isotope Laboratories, Inc.), methanol (Fischer-Scientific), ethanol (Pharmco-AAPER), ethylene glycol (Fischer-Scientific), and D4-methanol (Cambridge Isotope Laboratories, Inc., 99.8%) were used without further purification. The excitation sources employed for Raman spectroscopy were the 514.5 nm line from a Coherent Innova 200 Ar ion laser. The spectra were collected using a Jobin-Yvon Ramanor

HG2-S Raman spectrometer with two 1800 grooves/mm gratings and a thermoelectrically cooled (-30 °C) photomultiplier tube detector. A scan speed of 2 cm^{-1}/s was employed for spectra shown. Spectra were obtained for the solid state of TMAO in a vacuum chamber, and time-resolved spectra of solid TMAO in the presence of vapor-phase solvent were obtained to qualitatively show the effects of micro-solvation of neat TMAO. A vacuum chamber, which connects to a liquid reservoir and vacuum, was developed and is shown in Figure 4.2. The chamber allows for the analysis of TMAO and D9-TMAO and other solid phase samples in an atmosphere of the experimenter's choice. In this case, a series of hydrogen bond donors including water, methanol, ethanol, and ethylene glycol were employed in the studies of micro-solvation of neat TMAO.

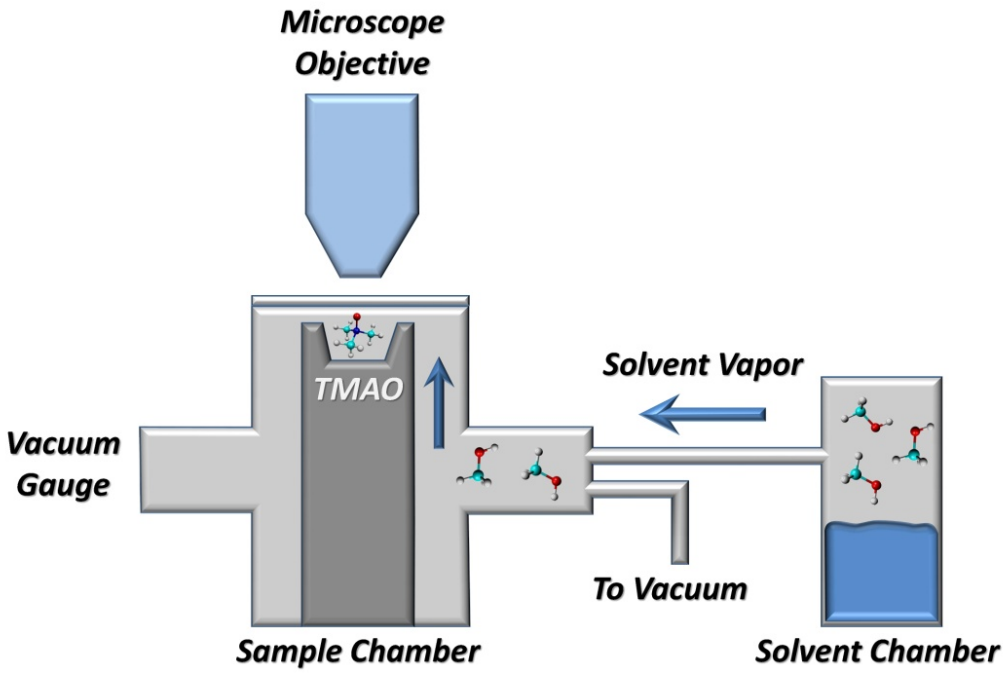

Figure 4.2. Custom Raman spectroscopy setup. Solvent vapor is introduced to solid phase TMAO in vacuum.

Theoretical Methods. Geometry optimizations and frequency calculations were performed on a 16-core Quantum Cube from Parallel Quantum Solutions using the *PQS* ab initio program package version 3.314 by Prof. David Magers.[99] Optimum equilibrium geometries and corresponding electronic energies of TMAO and TMAO with methanol, ethanol, and ethylene glycol molecules were determined using density functional theory.[25-26] The B3LYP hybrid functional comprising Becke's three parameter functional[22] using the LYP correlation functional of Lee, Yang, and Parr[23], with the augmented correlation consistent basis set aug-cc-pVTZ by Dunning and co-workers was utilized.[27-28] The vibrational frequencies of pure TMAO, D9-TMAO, methanol, D4-methanol, and TMAO with two methanol molecules were also calculated anharmonically using the *Gaussian 09* software package[100] with the MP2 method and the aug-cc-pVTZ and aug-cc-pVDZ basis set to aid in the assignment of fundamentals and combination bands in TMAO's and methanol's C-H stretching region. Natural bond orbital (NBO) calculations were performed on TMAO, methanol, and select molecular clusters using the *Gaussian 09* software package[100] using the B3LYP method and aug-cc-pVTZ basis set. Simulated spectra were constructed with a custom program developed with National Instruments *LabView*.

4.4 SPECTROSCOPIC RESULTS

TMAO is a very hygroscopic molecule and quickly forms a thin layer of water in a humid atmosphere.[49] In fact, many earlier vibrational spectroscopic investigations involving TMAO were complicated by this phenomenon. Here, spectra were acquired in a specially designed vacuum chamber in the presence of water, methanol, ethanol, and ethylene glycol vapor. Shown in Figures 4.3, 4.4, 4.5, and 4.6 are Raman spectra of TMAO in the presence of increasing amounts of water, methanol, ethanol, and ethylene glycol, respectively. Raman spectra of pure liquid water, methanol, ethanol, and ethylene glycol are included for comparison.

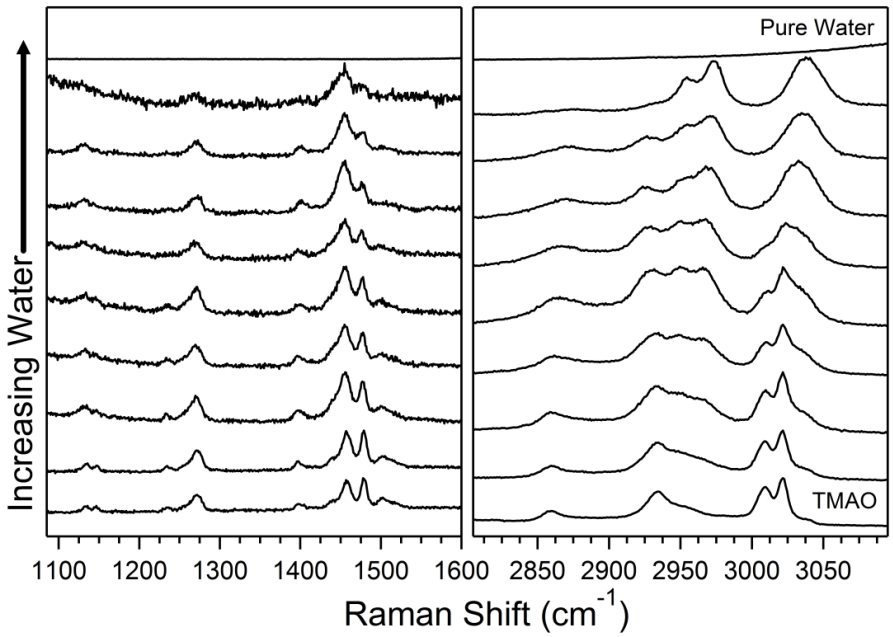

Figure 4.3. Raman spectra of solid anhydrous TMAO during microsolvation with water. The bottom spectrum is anhydrous TMAO in vacuum.

In the C-H stretching region of anhydrous TMAO (shown in Figure 4.3), there are three sets of peaks that evolve with increasing hydration. The highest energy doublet residing at just greater than 3000 cm^{-1} in anhydrous TMAO slowly converges into a broad single feature that is blue shifted in comparison to the original doublet. This final peak at 3030 cm^{-1} is the highest intensity peak in this region. A small peak at about ~3038 cm^{-1} steadily emerges with hydration and merges into this feature. The emergence of this new peak at 3038 cm^{-1} is the spectral signature of solvation.[49] The second set of peaks of interest in the C-H stretching region involve a prominent peak at 2930 cm^{-1} and two overlapped peaks starting at approximately ~2955 cm^{-1}. With hydration, the prominent peak at 2930 cm^{-1} decreases in intensity and red shifts to lower energy as the overlapped peaks increase in intensity, separate, and blue shift to final spectral positions at 2962 and 2974 cm^{-1}. The peak at 2860 cm^{-1} in anhydrous TMAO slowly broadens and slightly blue shifts with solvation. The C-H bending region of TMAO is also characterized by three sets of peaks. The prominent doublet at 1455 cm^{-1} and 1479 cm^{-1} increasingly red shift and collapses into one feature at 1450 cm^{-1}. A nearby small peak at 1500 cm^{-1} also disappears with solvation. Interestingly, the peak 1270 cm^{-1} only decreases slightly in intensity, but does not shift. The small doublet between 1125 and 1150 cm^{-1} gradually red shifts and collapses into one feature at 1130 cm^{-1}.

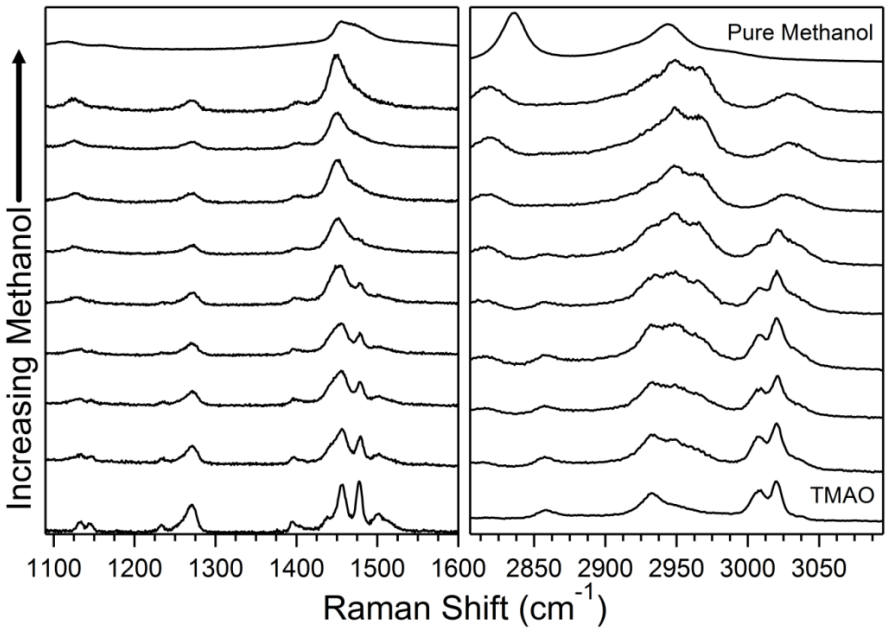

Figure 4.4. Raman spectra of solid anhydrous TMAO during microsolvation with methanol compared to the spectrum of pure methanol.

The spectra of TMAO when microsolvated by methanol, ethanol, and ethylene glycol exhibit many similarities to that of TMAO microhydrated with water. Both the C-H stretching and bending regions of TMAO are similarly affected by all three alcohols. The overall structure of TMAO becomes less pronounced as more solvent is deposited, with the two main doublets at approximately 1450 and 3000 cm^{-1} becoming single features, as in the case of water. Additional Raman features of all three alcohols themselves also contribute to the overall Raman spectra. There are some noticeable differences, however, between TMAO's spectrum hydrated with water and solvated with the three organic molecules, especially in the C-H stretching region. In the case of methanol microsolvation (Figure 4.4), a peak at 2815 cm^{-1} attributed to methanol slowly enters and intensifies with increasing microsolvation. Also, whereas in the case of water microhydration, the peak at 2860 cm^{-1} blue shifts, this is not the case with methanol, ethanol, or ethylene glycol. In methanol, ethanol, and ethylene glycol, it does not shift at all. Unfortunately, there are many possible overtones and combination bands that can account for this peak. In the C-H bending region all of the features behave similarly with microsolvation.

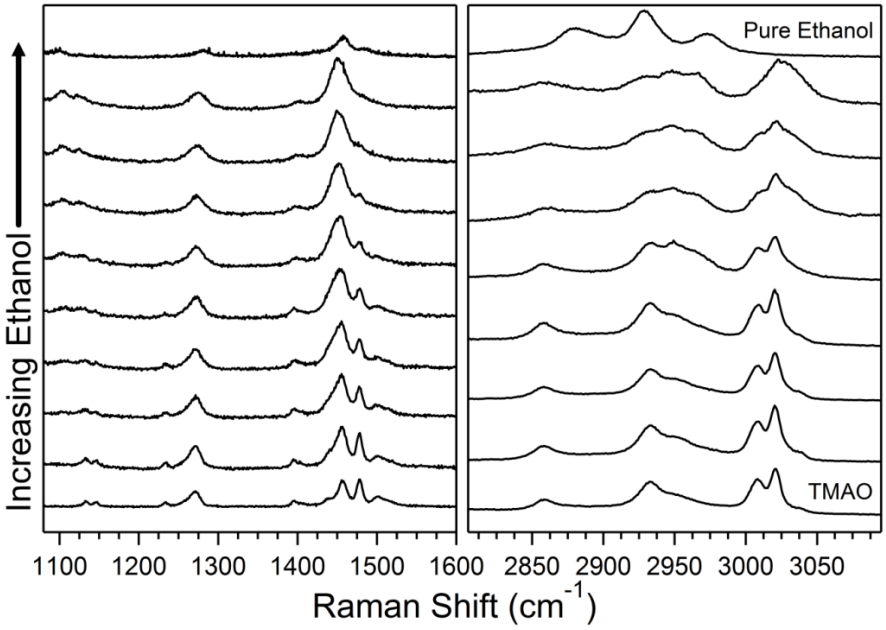

Figure 4.5. Raman spectra of solid anhydrous TMAO during microsolvation with ethanol compared to the spectrum of pure ethanol.

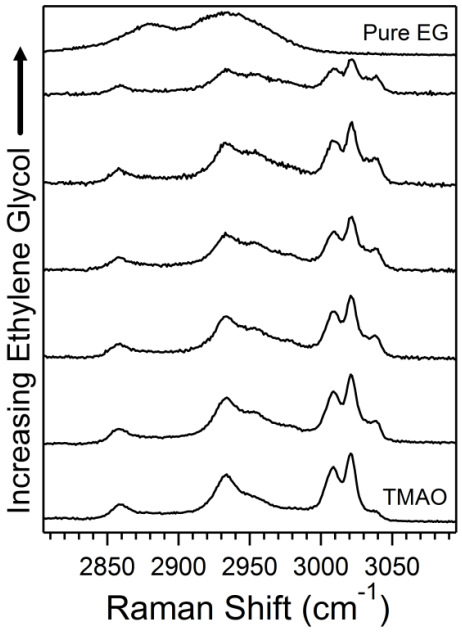

Figure 4.6. Raman spectra of solid anhydrous TMAO during microsolvation with ethylene glycol (EG) compared to the spectrum of pure ethylene glycol.

4.5 THEORETICAL RESULTS

Shown in Figures 4.7, 4.8, and 4.9 are optimized molecular structures of TMAO/methanol, TMAO/ethanol, and TMAO/ethylene glycol clusters as well as their corresponding simulated Raman spectra. In each case, one or more alcohol molecules hydrogen bond to TMAO's oxygen atom. Table 4.1 shows the energies of each of the clusters as well as their relative energies to each other. The table, as well as each of the simulated spectra, is ordered with increasing number of alcohol molecules attached to TMAO and increasing relative energy. In the case of methanol (Figure 4.7), structures with two hydrogen bonds to the oxygen atom of TMAO generally are more stable, although this is not the case with 4M-A, which has three hydrogen bonds and is 2.01 kcal/mol lower in energy than 4M-B, which has two hydrogen bonds to oxygen. The opposite is true in the case of ethanol and ethylene glycol, however. In ethanol, structures with one hydrogen bond to the oxygen atom of TMAO tend to be more stable than those with two hydrogen bonds. Structure 1E-C is much higher in energy than other structures due to the fact that instead of ethanol hydrogen bonding with the oxygen on TMAO, TMAO is hydrogen bonding to the oxygen in ethanol via TMAO's methyl groups. Interestingly, in ethylene glycol, structures with the fewest number of hydrogen bonds to TMAO's oxygen atom are the most stable.

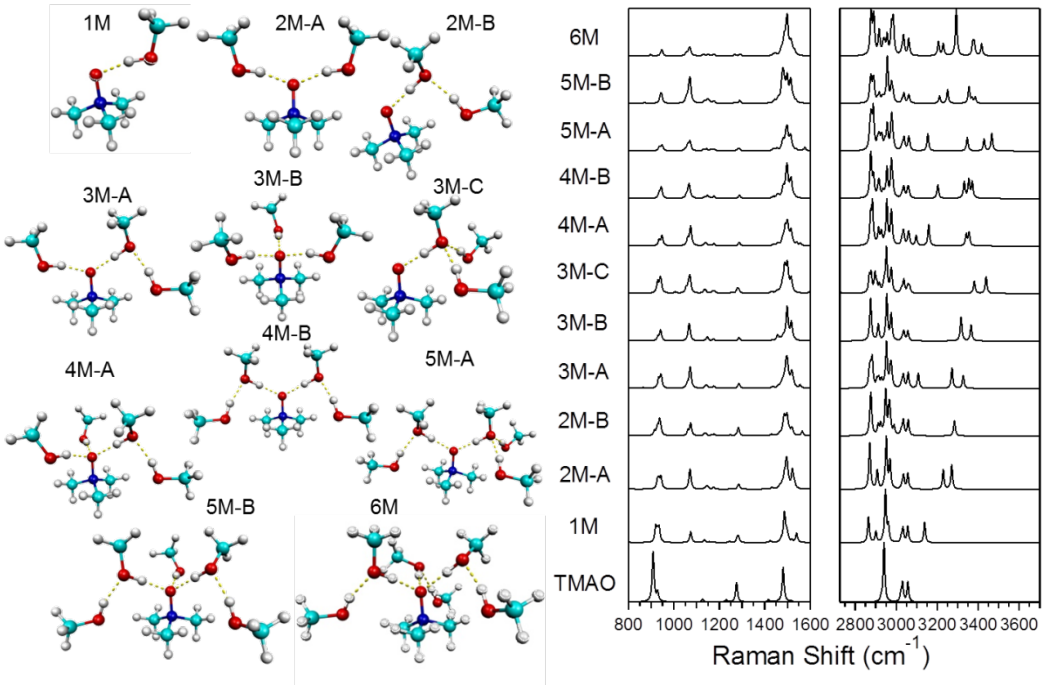

Figure 4.7. Optimized structures of TMAO with 1 to 6 methanol molecules as well as the corresponding simulated Raman spectra compared to an isolated TMAO molecule.

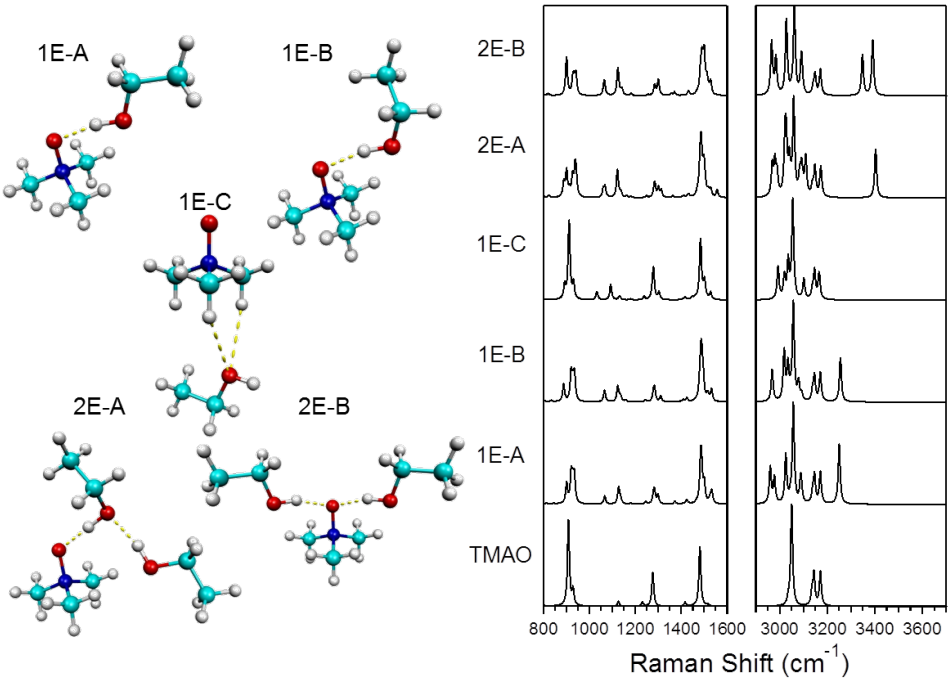

Figure 4.8. Optimized structures of TMAO with 1 or 2 ethanol molecules as well as the corresponding simulated Raman spectra compared to an isolated TMAO molecule.

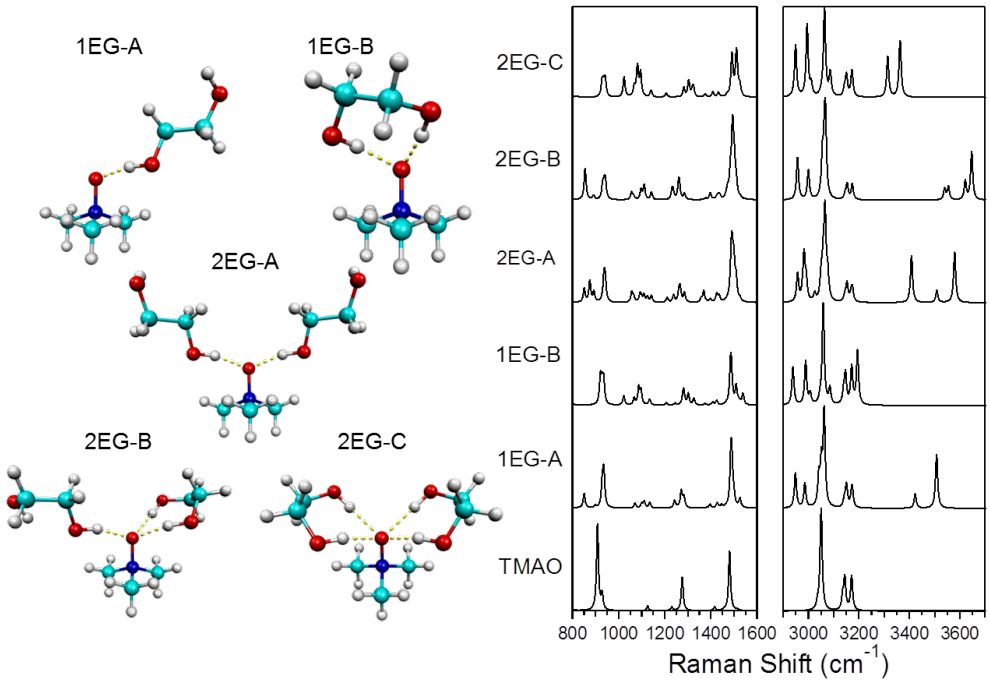

Figure 4.9. Optimized structures of TMAO with 1 or 2 ethylene glycol molecules as well as the corresponding simulated Raman spectra compared to an isolated TMAO molecule.

Table 4.1. Computed Energies, Zero Point Energies, and Relative Energies for TMAO and Microsolvated Clusters.

Structure	Energy (au)	Zero Point Energy (au)	ZPE Corrected (au)	Relative Energy (kcal/mol)
TMAO	-249.72179	0.125	-249.59679	-
1M	-365.52520	0.178	-365.34720	-
2M-A	-481.30944	0.232	-481.07744	0.00
2M-B	-481.30301	0.232	-481.07101	4.04
3M-A	-597.09922	0.285	-596.81422	0.00
3M-B	-597.09821	0.285	-596.81321	0.63
3M-C	-597.09351	0.284	-596.80951	2.95
4M-A	-712.89306	0.338	-712.55506	0.00
4M-B	-712.88985	0.338	-712.55185	2.01
5M-A	-828.68207	0.391	-828.29107	0.00
5M-B	-828.68202	0.391	-828.29102	0.03
6M	-944.47290	0.444	-944.02890	-
1E-A	-404.84602	0.206	-404.64002	0.00
1E-B	-404.84698	0.207	-404.63998	0.02
1E-C	-404.82784	0.205	-404.62284	10.80
2E-A	-559.97671	0.288	-559.68871	0.00
2E-B	-559.97531	0.288	-559.68731	0.88
1EG-A	-480.10155	0.213	-479.88855	0.00
1EG-B	-480.09242	0.211	-479.88142	4.48
2EG-A	-710.46789	0.300	-710.16789	0.00
2EG-B	-710.46600	0.301	-710.16500	1.81
2EG-C	-710.46030	0.298	-710.16230	3.51

4.6 DEUTERATED SPECTROSCOPIC AND ANHARMONIC THEORETICAL RESULTS

Due to overlap of spectral features upon microsolvation, especially in the C-H stretching region, the micro-solvation spectra of TMAO with D4-methanol and also D9-TMAO with H4-methanol were acquired and are shown in Figures 4.10 and 4.11, respectively. In addition, anharmonic frequency calculations on methanol, D4-methanol, TMAO, and D9-TMAO were performed and compared to experimental Raman spectra in order to aid in assignment of normal modes in these molecules. These results are shown in Figure 4.12. Table 4.2 lists a number of predicted combination bands and overtones that could account for the additional peaks in the experimental C-H and C-D stretching spectra.

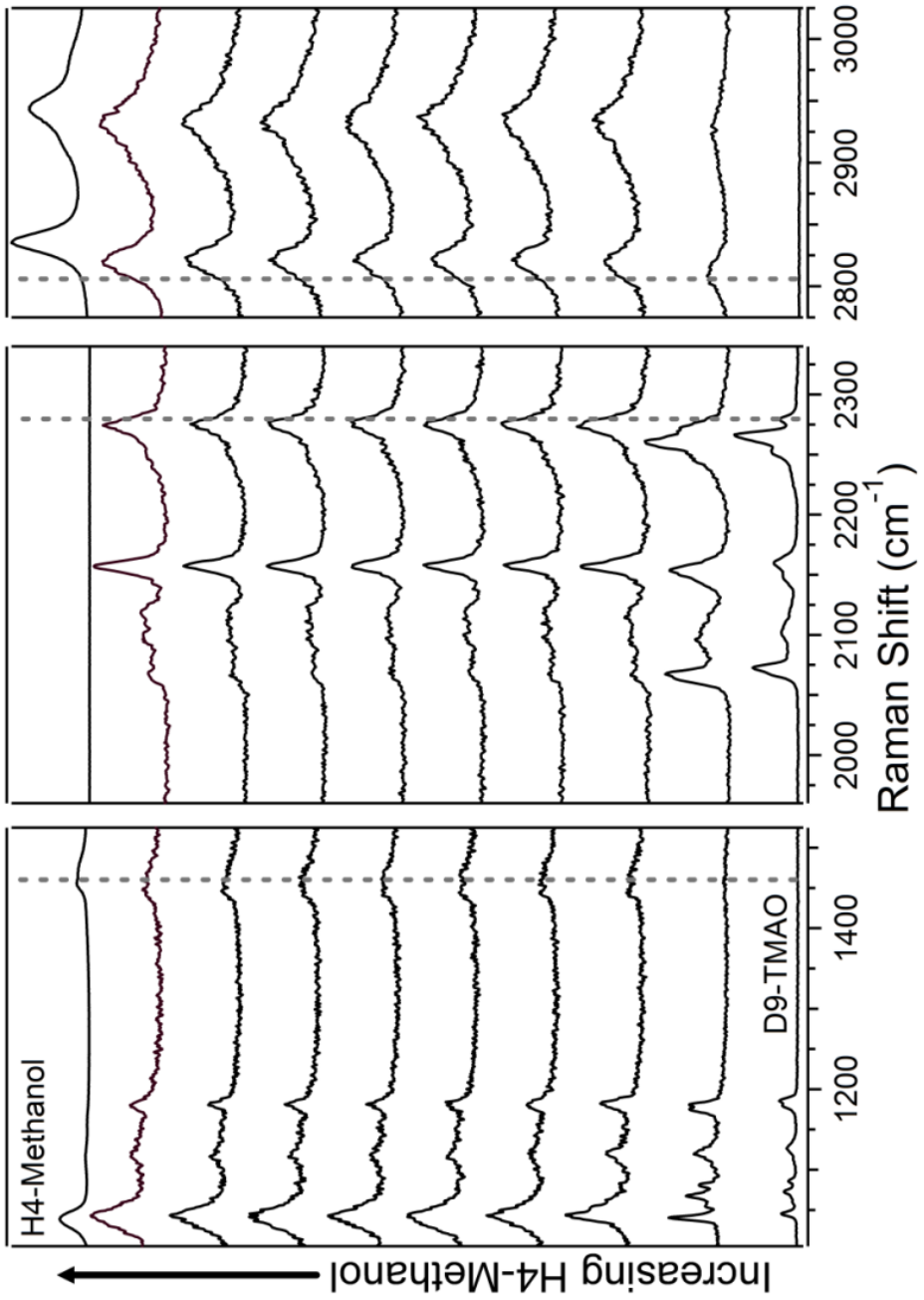

Figure 4.10. Raman spectra of solid anhydrous D9-TMAO during microsolvation with H4-methanol compared to the spectrum of pure methanol. The bottom spectrum is D9-TMAO in air. The appearance of the small feature at 2280 cm^{-1} indicates slight exposure to water vapor prior to study.

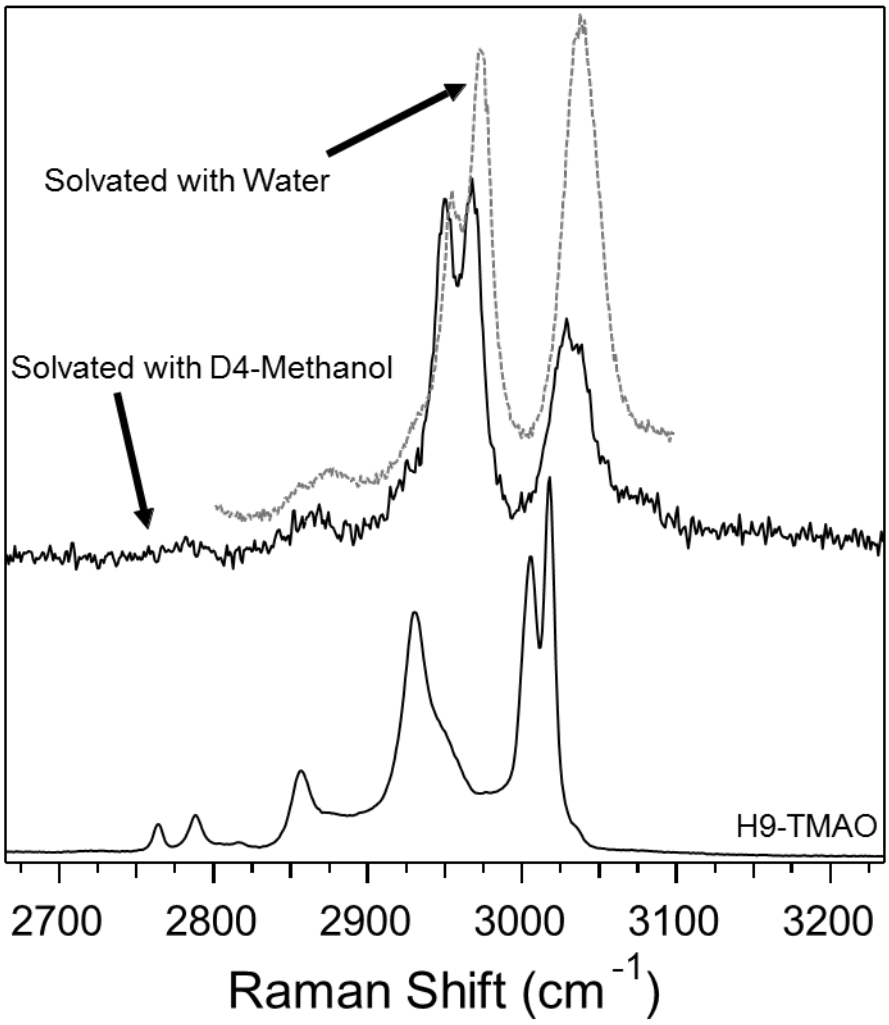

Figure 4.11. Raman spectra of solid anhydrous H9-TMAO compared to TMAO solvated with D4-methanol (solid curve) and water (dotted curve).

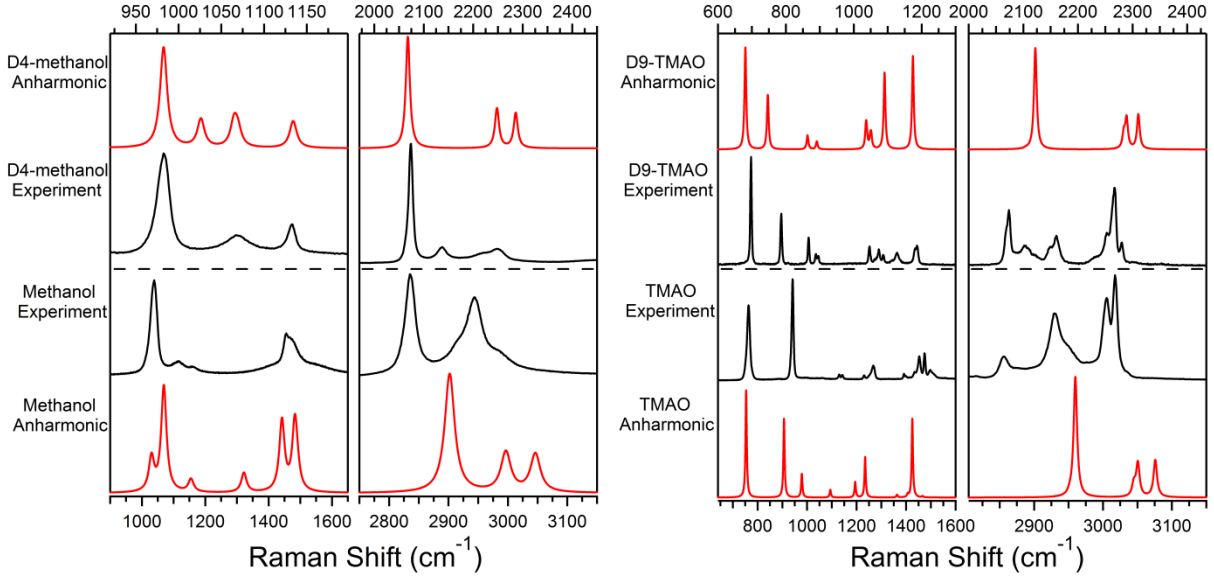

Figure 4.12. Comparison of the experimental (black) Raman spectra of methanol and D4-methanol (left) and TMAO and D9-TMAO (right) to the simulated (red) results of anharmonic frequency calculations.

Table 4.2. Possible overtone and combination bands predicted by anharmonic calculations performed at the MP2/aug-cc-pVTZ level to aid in the assignment of the experimental mode at 2860 cm^{-1} in TMAO's spectra (left), C-D stretching modes of D4-methanol (center) and C-H stretching modes of H4-methanol (right).

Mode(s) TMAO[49]	Frequency (cm^{-1})	Mode(s) MeOD[101]	Frequency (cm^{-1})	Mode(s) MeOH[101]	Frequency (cm^{-1})
3	2937	10	2144	3	2849
16	2882	6	2127	5 + 10	2806
17	2842	4	2064	7 + 3	2914
4 + 3	2873	6 + 4	2202	7 + 10	2800
16 + 3	2908	10 + 4	2198	3 + 5	2923
17 + 3	2889	10 + 6	2127		
16 +16	2885	5 + 4	2161		

4.7 NATURAL BONDING ORBITALS (NBO) RESULTS

Tables 4.3 and 4.4 list the changes in NBO populations (in me^-)[102-103] for methanol and TMAO in the 2M-A structure and water and TMAO for our previously reported 3W-B structure, respectively, relative to the individual non-interacting molecules. The largest change in the case of methanol comes in methanol's O-H σ* orbital, which gains 42 me^- per methanol molecule, and at the same time, TMAO's oxygen lone pairs and C-N σ* orbitals lose electron density. Methanol's C-H σ* orbitals also exhibit a slight increase in electron population. A similar effect is observed in the case of water where 35 me^- are gained by each water's O-H σ* orbital. The net effect in the 3W-B structure[49] is larger due to the presence of three water molecules.

Table 4.3. Population changes (in me^-) of the B3LYP/aug-cc-pVTZ NBOs of methanol and TMAO from the 2M-A structure relative to the non-interacting molecules.

Methanol			TMAO					
Orbital		Δq (me-)	Orbital		Δq (me-)	Orbital		Δq (me-)
σ	(O1 H2)	-2	σ	(O1 N2)	-2	n	(O1)	-24
σ	(O1 C3)	0	σ	(N2 C3)	0	σ*	(O1 N2)	7
σ	(C3 H4)	-1	σ	(N2 C7)	0	σ*	(N2 C3)	-11
σ	(C3 H5)	1	σ	(N2 C11)	0	σ*	(N2 C7)	-9
σ	(C3 H6)	-1	σ	(C3 H4)	-1	σ*	(N2 C11)	-11
n	(O1)	-6	σ	(C3 H5)	-1	σ*	(C3 H4)	0
n	(O1)	-8	σ	(C3 H6)	-2	σ*	(C3 H5)	1
σ*	(O1 H2)	42	σ	(C7 H8)	-1	σ*	(C3 H6)	-3
σ*	(O1 C3)	2	σ	(C7 H9)	-2	σ*	(C7 H8)	1
σ*	(C3 H4)	2	σ	(C7 H10)	-1	σ*	(C7 H9)	-3
σ*	(C3 H5)	1	σ	(C11 H12)	-2	σ*	(C7 H10)	1
σ*	(C3 H6)	2	σ	(C11 H13)	-1	σ*	(C11 H12)	-3
			σ	(C11 H14)	-1	σ*	(C11 H13)	1
			n	(O1)	-11	σ*	(C11 H14)	0
			n	(O1)	3			

Table 4.4. Population changes (in me^-) of the B3LYP/aug-cc-pVTZ NBOs of water and TMAO from the 3W-B[49] structure relative to the non-interacting molecules.

Water			TMAO					
Orbital		Δq (me^-)	Orbital		Δq (me^-)	Orbital		Δq (me^-)
σ	(H1 O2)	-2	σ	(O1 N2)	-2	n	(O1)	-7
σ	(O2 H3)	-1	σ	(N2 C3)	0	σ*	(O1 N2)	11
n	(O2)	-1	σ	(N2 C7)	0	σ*	(N2 C3)	-13
n	(O2)	-3	σ	(N2 C11)	0	σ*	(N2 C7)	-13
σ*	(H1 O2)	35	σ	(C3 H4)	-1	σ*	(N2 C11)	-13
σ*	(O2 H3)	1	σ	(C3 H5)	-1	σ*	(C3 H4)	0
			σ	(C3 H6)	-3	σ*	(C3 H5)	1
			σ	(C7 H8)	-1	σ*	(C3 H6)	-4
			σ	(C7 H9)	-3	σ*	(C7 H8)	0
			σ	(C7 H10)	-1	σ*	(C7 H9)	-4
			σ	(C11 H12)	-3	σ*	(C7 H10)	1
			σ	(C11 H13)	-1	σ*	(C11 H12)	-4
			σ	(C11 H14)	-1	σ*	(C11 H13)	0
			n	(O1)	-18	σ*	(C11 H14)	1
			n	(O1)	-7			

4. 8 DISCUSSION

Spectral shifts in the experimental microsolvated Raman spectra of TMAO interacting with the hydrogen bond donors methanol, ethanol, and ethylene glycol are very similar to those observed with water. This result suggests that interactions with TMAO's oxygen atom are dominating the local solvation geometry. Raman spectra of TMAO solvated with deuterated methanol (see Figure 4.11) allows for a direct comparison of the effects of solvation on TMAO's C-H stretching modes between water and methanol without spectral overlap with the CH stretches of methanol. We previously showed that the emergence of a new peak at 3038 cm^{-1} is the spectral signature of hydration of TMAO.[49] This feature is common to Raman spectra of TMAO solvated with all of the hydrogen bond donors studied here. In the comparison in Figure 4.11 of TMAO solvated with water and methanol, this peak is much more intense in the case of water. At the same time, the two overlapped peaks starting at 2955 cm^{-1} that increase in intensity, separate, and blue shift to final spectral positions of 2962 cm^{-1} and 2974 cm^{-1} in water also exhibit a different ratio in the case of methanol. These features stem from asymmetric C-H stretching motions in solvated TMAO and their blue-shifted positions are recovered by the theoretical results. The higher intensities of these blue-shifted features in the TMAO fully solvated with water suggest a more complete coverage of the solid TMAO's surface than in the case of methanol or other effects that are more pronounced with water than with methanol such as charge transfer between TMAO and the hydrogen bonded network.

The striking similarities in the Raman spectra of TMAO solvated with water and the solvents studied here suggest a common structural motif in all of the hydrogen bonded complexes. We previously showed that in the case of hydrogen bonding with water that a symmetric complex with three water molecules hydrogen bonded to TMAO's oxygen atom (see Figure 4.1) yielded

excellent agreement between experiment and theory. When TMAO is microsolvated by methanol, the lowest energy and more stable theoretical structures tend to correspond to TMAO molecules which are hydrogen bonded to two methanol molecules. This is similar to the case in liquid where methanol participates in on average 1.9 hydrogen bonds per molecule,[93] despite the fact that it is capable of forming three hydrogen bonds and on surfaces where methanol can only participate in two hydrogen bonds per molecule.[94] This is not the case with TMAO microsolvated by ethanol. In this case, the lowest energy structure that was identified exhibits bonding between TMAO and only one ethanol molecule with the second ethanol molecule preferring to hydrogen bond to the first ethanol molecule, rather than TMAO. This difference in stability could stem from the fact that the size of ethanol is twice that of methanol so that more methanol molecules are able to interact with TMAO.[92]

The best agreement between experiment and theory in the case of TMAO solvated with methanol comes from the theoretical structures 2M-A and 3M-B. Both of these methanol/TMAO structures have their methyl groups oriented away from TMAO's methyl groups and the hydrogen bonds are between the OH groups of the alcohol and the oxygen on TMAO. This is the same situation as we observed previously with water where TMAO was shown to hydrogen bond to three water molecules.[49] With ethanol, the theoretical structures in best agreement with experiment are the 1E-A and 1E-B structures with one ethanol molecule. These two structures are very close in energy with the 1E-A structure being slightly more stable. This structure orients the methyl groups of both the TMAO and the ethanol closer together than the 1E-B structure, which has the methyl groups oriented away from each other.

In the spectrum of TMAO and methanol that there is a methanol peak in the stretching region (2825 cm^{-1}) that is red shifted in comparison to pure methanol. This is shown in Figure 4.9 and

suggests that TMAO is affecting methanol's hydrogen bonded network. The fact that this peak red shifts confirms that methanol is acting as a hydrogen bond donor and is bonding to TMAO via the hydroxyl hydrogen.[79,81] The results of the NBO analysis on structure 2M-A reveal that the oxygen atom on TMAO experiences a decrease in electron population while the O-H σ* orbital of methanol experiences an almost equal but opposite increase in electron population upon complex formation. At the same time, there are small changes in methanol's C-H σ and σ* orbital populations. One C-H bond in methanol is a different length than the other two, and increases in electron population in the σ orbital as well as the σ* orbital, but to a lesser degree that the other C-H antibonding orbitals. The other two methyl bonds decrease in electron population in their σ bonding orbitals but increase in charge in the σ* orbitals. In addition to charge rearrangement, all three C-H bonds as well as the O-C bond in methanol elongate. The elongation of these bonds, as well as the increase in electron population of the σ* orbitals, is likely the origin of the observed experimental red shift of the C-H stretching mode at 2825 cm^{-1}. This hyperconjugation leads to a direct correlation between the charge transfers, change in bond distance, and observed shifts of vibrational modes.[103-105] A similar hyperconjugative effect is also observed in TMAO where one of the C-H bond lengths and orbital populations differs from the other two in each methyl group. This charge transfer is likely the origin of the blue shifting of TMAO's C-H stretching peaks.[49,105] The results of an NBO analysis on our previously reported 3W-B structure[49] reveals a similar effect in the case of water. Just as in the case of methanol, the C-H bonds in TMAO do not respond equally. However, the net transfer in the case of water is larger and is likely the origin of the greater blue shift and ratio of peaks observed in Figure 4.11.

The C-H (and C-D) stretching region of alcohols is complicated due to overlapping symmetric and asymmetric C-H stretching vibrations, Fermi resonances, and C-H bending overtones. [57,95] In methanol, the lower frequency peak (2830 cm^{-1}) has previously been attributed to the fundamental symmetric stretch[59,95,106-107] or a Fermi resonance[55,108-109] composed of a stretching fundamental and a bending overtone. The assignment of the second peak in methanol's C-H stretching region is also under debate, being attributed to either the asymmetric stretch[59,110-112] or the previously described Fermi resonance. A recent study suggested that the two peaks at 2830 cm^{-1} and 2950 cm^{-1} are involved in a Fermi resonance of the symmetric ν_3 mode and a bending overtone or combination band. The lower frequency peak was suggested to consist of a mixture of the ν_3 symmetric stretch, the ν_5 symmetric deformation, and two asymmetric deformations, ν_4 and ν_{10}; while the higher frequency peak consists of a mixture of the ν_3 symmetric stretch and the ν_5 symmetric deformation.[57] The anharmonic results presented here in Table 4.2 and Figure 4.12 suggest that the C-H stretching region does likely contain overtones and combination bands involving modes which correspond to bending motions of the C-H bonds. However, the excellent agreement shown in Figure 4.12 between the C-D bending and stretching spectra of D-4 methanol and the anharmonic fundamental results suggests that an overtone of the asymmetric deformation likely accounts for the appearance of the peak at 2133 cm^{-1} and that the other three fundamentals are mostly pure symmetric and asymmetric stretches. Taking this into account, the poor agreement between the experimental H4-methanol C-H stretching spectra and the anharmonic fundamental simulated spectrum suggests the peak at 2830 is participating in a Fermi resonance, likely with the overtone of the asymmetric deformation.

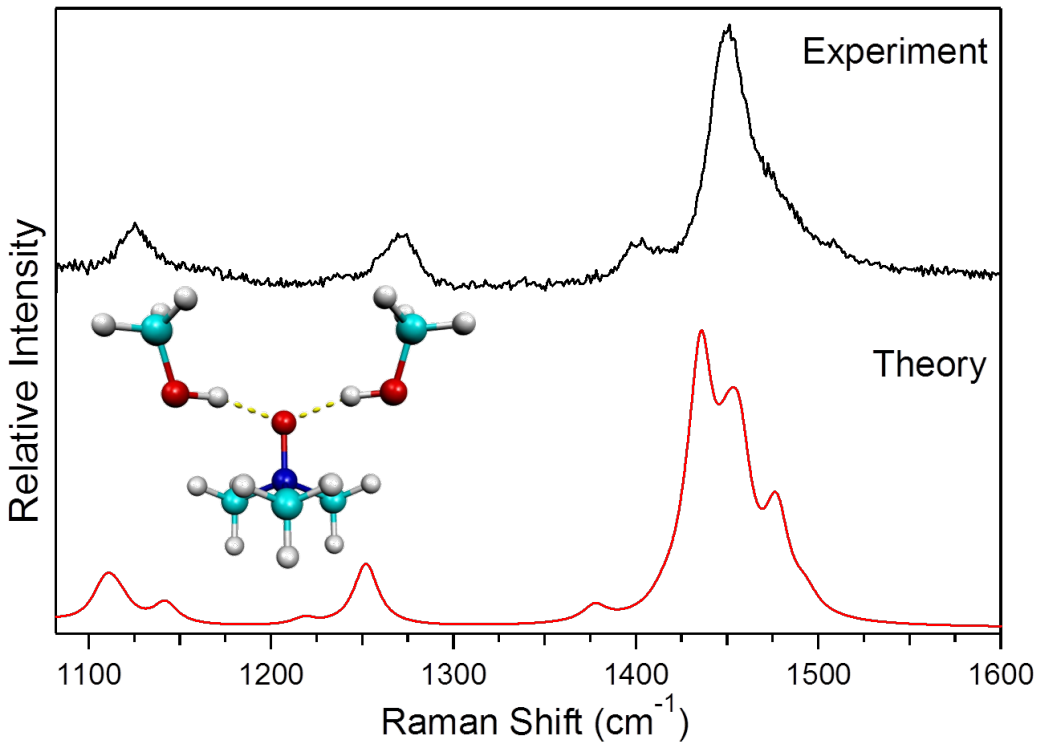

Figure 4.13. Comparison of the experimental (black) Raman spectra of the 2M-A structure to the simulated (red) results of anharmonic frequency calculations in the C-H bending region.

Figure 4.13 shows a comparison of the TMAO's Raman C-H bending spectrum when microsolvated with methanol to a simulated anharmonic vibrational spectrum performed at the MP2/aug-cc-PVDZ level on the 2M-A structure. The excellent agreement strongly suggests that TMAO is, on average, bonding to two methanol molecules. Anharmonic vibrational frequency calculations performed on the 2M-A structure for the C-H stretching region also confirm the red shift experimentally observed for methanol when hydrogen bonded to TMAO. Experimentally, the red shift for methanol's symmetric stretch is 18 cm^{-1} whereas the anharmonic calculation predicts a red shift of 21 cm^{-1}. Interestingly, one spectral feature in the Raman spectrum of TMAO that does not behave the same upon solvation is the feature at 2860 cm^{-1} in the C-H stretching region. This feature blue shifts and broadens when TMAO is microhydrated by water, but this is not the case with the alcohol solvents. The peak does not exhibit a shift when the solvent employed is methanol, ethanol, or ethylene glycol. The results of the anharmonic calculations (Table 4.2) suggest that a number of different overtones or combination bands could account for this peak, and the nature of this mode may explain the different behavior observed for water and alcohols. A definitive assignment of this mode, however, remains elusive.

4.9 CONCLUSIONS

The similarities in the Raman spectra of microsolvated TMAO using a variety of hydrogen bond donors suggest a common structural motif in all of the hydrogen bonded complexes. In particular, the arrangement of hydrogen bonds with TMAO's oxygen atom appears to dictate the extended hydrogen bonded network and is likely the origin of TMAO's osmolytic strength via the indirect effect. Hyperconjugation is observed in both TMAO and the hydrogen bonded solvent molecules. This charge transfer leads to blue shifts in TMAO's C-H stretching modes and a dramatic red shift in methanol's symmetric stretch. The effect is larger in the case of water and is likely the origin of TMAO's blue shifted C-H stretching modes in solution.

4.10 NOTE

This work was published in the *Journal of Physical Chemistry B* in December, 2014.[113]

BIBLIOGRAPHY

(1) *Lehninger: Principles of Biochemistry*.

(2) Pauling, L., *The Nature of the Chemical Bond*. Cornell University Press: Ithaca, NY, 1939.

(3) Pimental G.C., M. A. L., *The Hydrogen Bond*. Freeman: San Francisco, 1960.

(4) Pauling, L.; Corey, R. B.; Branson, H. R., The Structure of Proteins: Two Hydrogen-Bonded Helical Configurations of the Polypeptide Chain. *Proc. Natl. Acad. Sci. U. S. A.* **1951,** *37,* 205-11.

(5) Watson, J. D.; Crick, F. H. C., Molecular Structure of Nucleic Acids. A Structure for Deoxyribose Nucleic Acid. *Nature (London, U. K.)* **1953,** *171,* 737-8.

(6) Sturtevant, J. M., Heat Capacity and Entropy Changes in Processes Involving Proteins. *Proc. Natl. Acad. Sci. USA* **1977,** *74,* 2236-2240.

(7) Edsall, J. T., Apparent Molal Heat Capacities of Amino Acids and Other Organic Compounds. *J. Am. Chem. Soc.* **1935,** *57,* 1506-1507.

(8) Dill, K. A., Dominant Forces in Protein Folding. *Biochemistry* **1990,** *29,* 7133-7155.

(9) Spolar, R. S.; Ha, J.-H.; M. Thomas Record, J., Hydrophobic Effect in Protein Folding and Other Noncovalent Processes Involving Proteins. *Proc. Natl. Acad. Sci. U. S. A.* **1989,** *86,* 8382-8385.

(10) Privalov, P. L.; Gill, S. J., Stability of Protein Structure and Hydrophobic Interaction. *Adv. Protein Chem.* **1988,** *39,* 191-234.

(11) Eley, D. D.; Evans, M. G., Heats and Entropy Changes Accompanying the Solution of Ions in Water. *Transactions of the Faraday Society* **1938,** *34,* 1093-1112.

(12) Eley, D. D., On the Solubility of Gases. Part I. - The Inert Gases in Water. *Transactions of the Faraday Society* **1939,** *35,* 1281-1293.

(13) Eley, D. D., On the Solubility of Gases. Part II. - A Comparison of Organic Solvents with Water. *Transactions of the Faraday Society* **1939,** *35,* 1421-1432.

(14) Kauzmann, W., Adv. Protein Chem. *Adv. Protein Chem.* **1959,** *14,* 1.

(15) Frank, H. S.; Evans, M. W. J., Free Volume and Entropy in Condensed Systems III. Entropy in Binary Liquid Mixtures; Partial Molal Entropy in Dilute Solutions; Structure and Thermodynamics in Aqueous Electrolytes. *J. Chem. Phys.* **1945,** *13,* 507-533.

(16) Chandler, D., Interfaces and the Driving Force of Hydrophobic Assembly. *Nature* **2003**.

(17) Ballal, D.; Chapman, W. G., Hydrophobic and Hydrophilic Interactions in Aqueous Mixtures of Alcohols at a Hydrophobic Surface. *J. Chem. Phys.* **2013,** *139,* 114706-114717.

(18) Rezus, Y. L. A.; Bakker, H. J., Observation of Immobilized Water Molecules around Hydrophobic Groups. *Phys. Rev. Lett.* **2007,** *99,* 148301-148304.

(19) Galamba, N., Water's Structure around Hydrophobic Solutes and the Iceberg Model. *J. Phys. Chem. B* **2013,** *117,* 2153-2159.

(20) Di Michele, A.; Freda, M.; Onori, G.; Paolantoni, M.; Santucci, A.; Sassi, P., Modulation of Hydrophobic Effect by Cosolutes. *J. Phys. Chem. B* **2006,** *110,* 21077-21085.

(21) Engel, T.; Reid, P., *Physical Chemistry*. 3 ed.; Pearson 2013.

(22) Becke, A. D., Density-Functional Thermochemistry. III. The Role of Exact Exchange. *J. Chem. Phys.* **1993,** *98,* 5648-5652.

(23) Lee, C., Development of the Colle-Salvetti Correlation-Energy Formula into a Functional of the Electron Density. *Phys. Rev. B: Condens. Matter Mater. Phys.* **1988,** *37,* 785-789.

(24) Reed, A. E.; Curtiss, L. A.; Weinhold, F., Intermolecular Interactions from a Natural Bond Orbital, Donor-Acceptor Viewpoint. *Chem. Rev.* **1988,** *88,* 899-926.

(25) Hohenberg, P., Inhomogeneous Electron Gas. *Phys. Rev.* **1964,** *136,* B864-B871.

(26) Kohn, W., Self-Consistent Equations Including Exchange and Correlation Effects. *Phys. Rev.* **1965,** *140,* A1133-A1138.

(27) Dunning Jr, T. H., Gaussian Basis Sets for Use in Correlated Molecular Calculations. I. The Atoms Boron through Neon and Hydrogen. *J. Chem. Phys.* **1989,** *90,* 1007-1023.

(28) Kendall, R. A., Electron Affinities of the First-Row Atoms Revisited. Systematic Basis Sets and Wave Functions. *J. Chem. Phys.* **1992,** *96,* 6796-6806.

(29) Bolen, D. W.; Rose, G. D., Structure and Energetics of the Hydrogen-Bonded Backbone in Protein Folding. *Annu. Rev. Biochem* **2008,** *77,* 339-362.

(30) Zhang, Y. J.; Cremer, P. S., Chemistry of Hofmeister Anions and Osmolytes. *Annu. Rev. Phys. Chem.* **2010,** *61,* 63-83.

(31) Attri, P.; Venkatesu, P.; Lee, M.-J., Influence of Osmolytes and Denaturants on the Structure and Enzyme Activity of A-Chymotrypsin. *J. Phys. Chem. B* **2010,** *114,* 1471-1478.

(32) Canchi, D. R.; García, A. E., Cosolvent Effects on Protein Stability. *Annu. Rev. Phys. Chem.* **2013,** *64,* 273-293.

(33) Kuffel, A., The Hydrogen Bond Network Structure within the Hydration Shell around Simple Osmolytes: Urea, Tetramethylurea, and Trimethylamine-N-Oxide, Investigated Using Both a Fixed Charge and a Polarizable Water Model. *J. Chem. Phys.* **2010,** *133,* 035102-035109.

(34) Wei, H.; Fan, Y.; Gao, Y. Q., Effects of Urea, Tetramethyl Urea, and Trimethylamine N-Oxide on Aqueous Solution Structure and Solvation of Protein Backbones: A Molecular Dynamics Simulation Study. *J. Phys. Chem. B* **2010,** *114,* 557-568.

(35) Kocherbitov, V.; Veryazov, V.; Soderman, O., Hydration of Trimethylamine-N-Oxide and of Dimethyldodecylamine-N-Oxide: An Ab Initio Study. *J. Mol. Struct. (THEOCHEM)* **2007,** *808,* 111-118.

(36) Maclagan, R.; Malardier-Jugroot, C.; Whitehead, M. A.; Lever, M., Theoretical Studies of the Interaction of Water with Compensatory and Noncompensatory Solutes for Proteins. *J. Phys. Chem. A* **2004,** *108,* 2514-2519.

(37) Linton, E. P., The Dipole Moments of Amine Oxides. *J. Am. Chem. Soc.* **1940,** *62,* 1945-1948.

(38) Armstrong, R. S.; Aroney, M. J.; Calderbank, K. E.; Pierens, R. K., Molar Kerr Constants and Solute Polarizability Anisotropies of Ammonia, Trimethylamine, Trimethylamine Oxide and 1,4-Diazabicyclo[2.2.2]Octane. *Aust. J. Chem.* **1977,** *30,* 1411-15.

(39) Phillips, G. M.; Hunter, J. S.; Sutton, L. E., An Investigation of the Occurrence of the Co-Ordinate or Dative Link by Electric Dipole-Moment Measurements. *J. Chem. Soc.* **1945,** 146-162.

(40) Tsygankova, N. G.; Bubel, O. N.; Grinshpan, D. D.; Kaputskii, F. N., Mndo Calculation of Steric and Electronic Structure of Molecules of Tertiary Amine Oxides. *Vestsi Akad. Navuk BSSR, Ser. Khim. Navuk* **1988,** 35-37.

(41) Yakimanskii, A. V.; Bochek, A. M.; Zubkov, V. A.; Petropavlovskii, G. A., Quantum-Chemical Analysis of the Electronic Structure of Solvents for Cellulose (Amine Oxides). *Zh. Prikl. Khim. (Leningrad)* **1991,** *64,* 622-626.

(42) Kast, K. M.; Brickmann, J.; Kast, S. M.; Berry, R. S., Binary Phases of Aliphatic N-Oxides and Water: Force Field Development and Molecular Dynamics Simulation. *J. Phys. Chem. A* **2003,** *107,* 5342-5351.

(43) Kast, K. M.; Reiling, S.; Brickmann, J., Ab Initio Investigations of Hydrogen Bonding in Aliphatic N-Oxide-Water Systems. *J. Mol. Struct. (THEOCHEM)* **1998,** *453,* 169-180.

(44) Saladino, G., A Simple Mechanism Underlying the Effect of Protecting Osmolytes on Protein Folding. *J. Chem. Theory Comput.* **2011,** *7,* 3846-3852.

(45) Hunger, J., Complex Formation in Aqueous Trimethylamine-N-Oxide (TMAO) Solutions. *J. Phys. Chem. B* **2012,** *116,* 4783-4795.

(46) Rogachev, A. Y., Bonding Situation and NO-Bond Strengths in Amine-N-Oxides-A Combined Experimental and Theoretical Study. *physical Chemistry Chemical Physics (Incorporating Faraday Transactions)* **2012,** *14,* 1985-2000.

(47) Zou, Q.; Bennion, B. J.; Daggett, V.; Murphy, K. P., The Molecular Mechanism of Stabilization of Proteins by Tmao and its Ability to Counteract the Effects of Urea. *J. Am. Chem. Soc.* **2002,** *124,* 1192-1202.

(48) Tanford, C., The Hydrophobic Effect. Wiley: New York, 1980.

(49) Munroe, K. L.; Hammer, N. I.; Magers, D., Raman Spectroscopic Signatures of Noncovalent Interactions between Trimethylamine N-Oxide (TMAO) and Water. *J. Phys. Chem. B* **2011,** *115,* 7699-7707.

(50) Shibukawa, M.; Kondo, Y.; Ogiyama, Y.; Osuga, K.; Saito, S., Interfacial Water on Hydrophobic Surfaces Recognized by Ions and Molecules. *Phys. Chem. Chem. Phys.* **2011,** *13,* 15925-15935.

(51) Scatena, L. F.; Brown, M. G.; Richmond, G. L., Water at Hydrophobic Surfaces: Weak Hydrogen Bonding and Strong Orientation Effects. *Science (Washington, DC, U.S.)* **2001,** *292,* 908-912.

(52) Tarbuck, T. L.; Ota, S. T.; Richmond, G. L., Spectroscopic Studies of Solvated Hydrogen and Hydroxide Ions at Aqueous Surfaces. *J. Am. Chem. Soc.* **2006,** *128,* 14519-14527.

(53) Gopalakrishnan, S.; Liu, D.; Allen, H. C.; Kuo, M.; Shultz, M. J., Vibrational Spectroscopic Studies of Aqueous Interfaces: Salts, Acids, Bases, and Nanodrops. *ChemInform* **2006,** *37*.

(54) Rai, D., Methanol Clusters $(CH_3OH)N$, N = 3-6 in External Electric Fields: Density Functional Theory Approach. *J. Chem. Phys.* **2011,** *135,* 024307-024319.

(55) Ebukuro, T., Raman Spectroscopic Studies on Hydrogen Bonding in Methanol and Methanol/Water Mixtures under High Temperature and Pressure. *J. Supercrit. Fluids* **1999,** *15,* 73-78.

(56) Ahmed, M. K., The C-O Stretching Infrared Band as a Probe of Hydrogen Bonding in Ethanol-Water and Methanol-Water Mixtures. *Spectrosc. Lett.* **2012,** *45,* 420-423.

(57) Ishiyama, T.; Sokolov, V. V.; Morita, A., Molecular Dynamics Simulation of Liquid Methanol. Ii. Unified Assignment of Infrared, Raman, and Sum Frequency Generation Vibrational Spectra in Methyl C-H Stretching Region. *J. Chem. Phys.* **2011,** *134,* 024510-024520.

(58) Colles, M. J.; Griffiths, J. E., Relative and Absolute Raman Scattering Cross Sections in Liquids. *J. Chem. Phys.* **1972,** *56,* 3384-3391.

(59) Kamogawa, K.; Kitagawa, T., Solute/Solvent and Solvent/Solvent Interactions in Methanol Solutions: Quantitative Separation by Raman Difference Spectroscopy. *J. Phys. Chem.* **1985,** *89,* 1531-1537.

(60) Zhu, X.; Yao, J.; Li, H.; Han, S., Prediction among Different Spectroscopic Properties for Aqueous Systems. *J. Chem. Phys.* **2006,** *124,* 244501-244505.

(61) Kamogawa, K.; Kaminaka, S.; Kitagawa, T., Behavior of Ethanol in Various Binary Solutions: Difference Raman Spectroscopy on the C-H Stretching Vibrations. *J. Phys. Chem.* **1987,** *91,* 222-226.

(62) Cheng, T.; Sun, H., Adsorption of Ethanol Vapor on Mica Surface under Different Relative Humidities: A Molecular Simulation Study. *J. Phys. Chem. C* **2012**.

(63) Vartia, A. A., On the Reorientation and Hydrogen-Bond Dynamics of Alcohols. *J. Phys. Chem. B* **2011,** *115,* 12173-12178.

(64) Shao, Q., From Protein Denaturant to Protectant: Comparative Molecular Dynamics Study of Alcohol/Protein Interactions. *J. Chem. Phys.* **2012,** *136,* 115101-115109.

(65) Miura, Y., Nmr Studies on Thermal Stability of A-Helix Conformation of Melittin in Pure Ethanol and Ethanol-Water Mixture Solvents. . *J. Pept. Sci.* **2011,** *17,* 798-804.

(66) Reddy, Destruction of Hydrogen Bonds of Poly(N-Isopropylacrylamide) Aqueous Solution by Trimethylamine N-Oxide. *J. Chem. Phys.* **2012,** *136,* 234904-234913.

(67) Fileti, E. E., Calculated Infrared Spectra of Hydrogen-Bonded Methanol-Water, Water-Methanol, and Methanol-Methanol Complexes. *Int. J. Quantum Chem.* **2005,** *104,* 808-815.

(68) Freda, M.; Onori, G.; Santucci, A., Infrared and Dielectric Spectroscopy Study of the Water Perturbation Induced by Two Small Organic Solutes. *J. Mol. Struct.* **2001,** *565-566,* 153-157.

(69) Freda, M.; Onori, G.; Santucci, A., Infrared Study of the Hydrophobic Hydration and Hydrophobic Interactions in Aqueous Solutions of Tert-Butyl Alcohol and Trimethylamine-N-Oxide. *J. Phys. Chem. B* **2001,** *105,* 12714-12718.

(70) Freda, M.; Onori, G.; Santucci, A., Hydrophobic Hydration and Hydrophobic Interaction in Aqueous Solutions of Tert-Butyl Alcohol and Trimethylamine-N-Oxide: A Correlation with

the Effect of These Two Solutes on the Micellization Process. *Phys. Chem. Chem. Phys.* **2002,** *4,* 4979-4984.

(71) Kahovec, L., The Raman Spectrum of Trimethylamine Oxide. *Anz. Akad. Wiss. Wien Math. Naturw. Klasse* **1944,** *81,* 32-34.

(72) Kuroda, Y.; Kimura, M., Vibrational Spectra of Trimethylamine Oxide Dihydrate. *Spectrochim. Acta* **1966,** *22,* 47-56.

(73) Goubeau, J.; Fromme, I., Nitrogen-Oxygen Bond. I. Nitrogen-Oxygen Bonds without Mesomerism. *Z. Anorg. Chem.* **1949,** *258,* 18-26.

(74) Edsall, J. T., Raman Spectra of Amino Acids and Related Substances III. Ionization and Methylation of the Amino Group. *J. Chem. Phys.* **1937,** *5,* 225-237.

(75) Fileti, E. E., Calculations of Vibrational Frequencies, Raman Activities and Degrees of Depolarization for Complexes Involving Water, Methanol and Ethanol. *Chem. Phys. Lett.* **2008,** *452,* 54-58.

(76) Sun, Y.; Zheng, R.; Shi, Q., Theoretical Study of Raman Spectra of Methanol in Aqueous Solutions: Non-Coincident Effect of the CO Stretch. *J. Phys. Chem. B* **2012,** *116,* 4543-4551.

(77) Ahmed, M. K.; Ali, S.; Wojcik, E., The C-O Stretching Infrared Band as a Probe of Hydrogen Bonding in Ethanol-Water and Methanol-Water Mixtures. *Spectroscopy letters* **2012,** *45,* 420-423.

(78) Georgiev G.M., V. K., Gyamchev K. , Hydrogen Bonds in Water-Methanol Mixture. *Bulgarian Journal of Physics* **2007,** *34,* 103-107.

(79) Karpfen, A., Blue-Shifted A-H Stretching Frequencies in Complexes with Methanol: The Decisive Role of Intramolecular Coupling. *PCCP* **2011,** *13,* 14194-14201.

(80) Keefe, C. D.; Gillis, E. A. L.; MacDonald, L., Improper Hydrogen-Bonding CH·Y Interactions in Binary Methanol Systems as Studied by FTIR and Raman Spectroscopy. *J. Phys. Chem. A* **2009,** *113,* 2544-2550.

(81) Keefe, C. D.; Istvankova, Z., Computational Study of Proper and Improper Hydrogen Bonding in Methanol Complexes. *Can. J. Chem.* **2011,** *89,* 34-46.

(82) Hommel, E. L.; Merle, J. K.; Ma, G.; Hadad, C. M.; Allen, H. C., Spectroscopic and Computational Studies of Aqueous Ethylene Glycol Solution Surfaces. *J. Phys. Chem. B* **2004,** *109,* 811-818.

(83) Rutkowski, K. S.; Melikova, S. M.; Rospenk, M.; Koll, A., Strong and Weak Effects Caused by Non Covalent Interactions between Chloroform and Selected Electron Donor Molecules. *Phys. Chem. Chem. Phys.* **2011,** *13,* 14223-14234.

(84) Nedic, M.; Wassermann, T. N.; Larsen, R. W.; Suhm, M. A., A Combined Raman- and Infrared Jet Study of Mixed Methanol-Water and Ethanol-Water Clusters. *Phys. Chem. Chem. Phys.* **2011,** *13,* 14050-14063.

(85) Mandal, A.; Prakash, M.; Kumar, R. M.; Parthasarathi, R.; Subramanian, V., Ab Initio and DFT Studies on Methanol-Water Clusters. *J. Phys. Chem. A* **2010,** *114,* 2250-2258.

(86) Shimoaka, T.; Katsumoto, Y., Blue Shift of the Isolated CD Stretching Band of CH_2DOH in Water Induced by Changes in the Hydrogen-Bonding Pattern. *J. Phys. Chem. A* **2010,** *114,* 11971-11976.

(87) Lin, K.; Zhou, X.; Luo, Y.; Liu, S., The Microscopic Structure of Liquid Methanol from Raman Spectroscopy. *J. Phys. Chem. B* **2010,** *114,* 3567-3573.

(88) WU Bin, L. X.-s., LU Jian,NI Xiao-wu, Determination of Ethanol Concentration of Aqueous Solution by Using Raman Stretching Frequency Shifts. *China Academic Journal* **2010**.

(89) Dixit, S.; Crain, J.; Poon, W. C. K.; Finney, J. L.; Soper, A. K., Molecular Segregation Observed in a Concentrated Alcohol-Water Solution. *Nature* **2002,** *416,* 829-832.

(90) Pascal, T. A.; Goddard, W. A., Hydrophobic Segregation, Phase Transitions and the Anomalous Thermodynamics of Water/Methanol Mixtures. *J. Phys. Chem. B* **2012,** *116,* 13905-13912.

(91) Ghosh, M. K.; Uddin, N.; Choi, C. H., Hydrophobic and Hydrophilic Associations of a Methanol Pair in Aqueous Solution. *J. Phys. Chem. B* **2012,** *116,* 14254-14260.

(92) Siler, A. R.; Walker, R. A., Effects of Solvent Structure on Interfacial Polarity at Strongly Associating Silica/Alcohol Interfaces. *J. Phys. Chem. C* **2011,** *115,* 9637-9643.

(93) Andanson, J.-M., Relation between Hydrogen Bonding and Intramolecular Motions in Liquid and Supercritical Methanol. *J. Mol. Liq.* **2006,** *129,* 101-107.

(94) Baber, A. E.; Lawton, T. J.; Sykes, E. C. H., Hydrogen-Bonded Networks in Surface-Bound Methanol. *J. Phys. Chem. C* **2011,** *115,* 9157-9163.

(95) Stanners, C. D.; Du, Q.; Chin, R. P.; Cremer, P.; Somorjai, G. A.; Shen, Y. R., Polar Ordering at the Liquid-Vapor Interface of N-Alcohols (C1-C8). *Chem. Phys. Lett.* **1995,** *232,* 407-413.

(96) Choplin, F.; Kaufmann, G., Vibration Spectra and Normal Coordinate Analysis of Trimethylamine, Trimethylphosphine, and Trimethylarsine Oxides. *Spectrochim. Acta, Part A* **1970,** *26,* 2113-24.

(97) Giguere, P. A.; Chin, D., An Infrared Study of Trimethylamine Oxide, its Hydrate, and its Hydrochloride. *Can. J. Chem.* **1961,** *39,* 1214-1220.

(98) Mathis, R., Absorption Spectra of Some Tertiary Amine Oxides. *CR* **1956,** *242,* 1873-1876.

(99) *PQS Ab Initio Program Package*, Parallel Quantum Solutions: Fayetteville, Arkansas, 2007.

(100) Frisch, M.; Trucks, G.; Cheeseman, J.; Scalmani, G.; Clemente, F.; Caricato, M.; Patel, P.; Fox, D.; Morokuma, K.; Jacokowski, I., et al. *Gaussian*, Revision A.1; Gaussian, Inc.: Wallingford CT, 2009.

(101) Ishiyama, T.; Sokolov, V. V.; Morita, A., Molecular Dynamics Simulation of Liquid Methanol. I. Molecular Modeling Including C-H Vibration and Fermi Resonance. *J. Chem. Phys.* **2011,** *134,* 024509-024526.

(102) Howard, A. A.; Tschumper, G. S.; Hammer, N. I., Effects of Hydrogen Bonding on Vibrational Normal Modes of Pyrimidine. *J. Phys. Chem. A* **2010,** *114,* 6803-6810.

(103) Wright, A. M.; Howard, A. A.; Howard, J. C.; Tschumper, G. S.; Hammer, N. I., Charge Transfer and Blue Shifting of Vibrational Frequencies in a Hydrogen Bond Acceptor. *J. Phys. Chem. A* **2013,** *117,* 5435-5446.

(104) Chandra, A. K.; Parveen, S.; Zeegers-Huyskens, T., Anomeric Effects in the Symmetrical and Asymmetrical Structures of Triethylamine. Blue-Shifts of the C−H Stretching Vibrations in Complexed and Protonated Triethylamine. *J. Phys. Chem. A* **2007,** *111,* 8884-8891.

(105) Chandra, A. K.; Parveen, S.; Das, S.; Zeegers-Huyskens, T., Blue Shifts of the C-H Stretching Vibrations in Hydrogen-Bonded and Protonated Trimethylamine. Effect of Hyperconjugation on Bond Properties. *J. Comput. Chem.* **2008**.

(106) Ma, G.; Allen, H. C., Surface Studies of Aqueous Methanol Solutions by Vibrational Broad Bandwidth Sum Frequency Generation Spectroscopy. *J. Phys. Chem. B* **2003,** *107,* 6343-6349.

(107) Schwartz, M.; Moradi-Araghi, A.; Koehler, W. H., Fermi Resonance in Aqueous Methanol. *J. Mol. Struct.* **1980,** *63,* 279-285.

(108) Devendorf, G. S.; Hu, M.-H. A.; Ben-Amotz, D., Pressure Dependent Vibrational Fermi Resonance in Liquid CH_3OH and CH_2Cl_2. *J. Phys. Chem. A* **1998,** *102,* 10614-10619.

(109) Arencibia, A.; Taravillo, M.; Caceres, M.; Nunez, J.; Baonza, V. G., Pressure Tuning of the Fermi Resonance in Liquid Methanol: Implications for the Analysis of High-Pressure Vibrational Spectroscopy Experiments. *J. Chem. Phys.* **2005,** *123,* 214502-214510.

(110) Iwaki, L. K.; Dlott, D. D., Ultrafast Vibrational Energy Redistribution within C–H and O–H Stretching Modes of Liquid Methanol. *Chem. Phys. Lett.* **2000,** *321,* 419-425.

(111) Pogorelov, V.; Bulavin, L.; Doroshenko, I.; Fesjun, O.; Veretennikov, O., The Structure of Liquid Alcohols and the Temperature Dependence of Vibrational Bandwidth. *J. Mol. Struct.* **2004,** *708,* 61-65.

(112) Wang, C.-y.; Groenzin, H.; Shultz, M. J., Surface Characterization of Nanoscale Tio2 Film by Sum Frequency Generation Using Methanol as a Molecular Probe. *J. Phys. Chem. B* **2003,** *108,* 265-272.

(113) Cuellar, K. A.; Munroe, K. L.; Magers, D. H.; Hammer, N. I., Noncovalent Interactions in Microsolvated Networks of Trimethylamine N-Oxide. *The Journal of Physical Chemistry B* **2014,** *118,* 449-459.

VITA

Experience

University of Mississippi, University, MS

Graduate Research Associate	2012-Present
Undergraduate Research Associate	2011-2012

Education

University of Mississippi, University, MS

M.S. Physical Chemistry	2012-Present
B.A. Chemistry, Minors in Math and Spanish	2008-2012

Honors

University of Mississippi, University, MS

- Gamma Beta Phi Honor Society
- Phi Theta Kappa Honor Society
- University of Mississippi Dean's Honor Roll
- 2011-2012 ACS Undergraduate Research Award

Publications

Kristina A. Cuellar, Katherine L. Munroe, David H. Magers, and Nathan I. Hammer "Noncovalent Interactions in Microsolvated Networks of Trimethylamine *N*-oxide." *J. Phys. Chem. B*, **2014**, 118 (2), pp 449–459 DOI: 10.1021/jp408659n

G. E. Tyson, K. Tokmic, C. S. Oian, D. Rabinovich, H. U. Valle, T. K. Hollis, J. T. Kelly, **K. A. Cuellar**, L.E. McNamara, N. I. Hammer, C. E. Webster, A. G. Oliver, "Synthesis, Characterization, "Photophysical Properties, and Catalytic Activity of a SCS bis(N-heterocyclic thione) (SCS-NHT) Pd Pincer Complex," *Dalton Transactions*, submitted **(2014).**

Ashton Nicholson, **Kristina A. Cuellar**, David H. Magers, and Nathan I. Hammer "Noncovalent Interactions in Microhydrated Networks of Dimethyl Sulfoxide." *J. Phys. Chem. B*, to be submitted.

Professional Presentations (* represents the presenter)

Kristina A. Cuellar*, "Noncovalent Interactions in Microsolvated Networks of Trimethylamine N-Oxide (TMAO)," Seminar, University of Mississippi, University, MS, July 2014.

Kristina A. Cuellar*, Katherine L. Munroe, David H. Magers, and Nathan I. Hammer, "Noncovalent Interactions in Micro-Solvated Networks of Trimethylamine N-Oxide (TMAO)," Poster, 2014 Mississippi State EPSCoR Meeting, Starkville, MS, April 2014.

Ashton Nicholson*, **Kristina A. Cuellar**, David H. Magers, and Nathan I. Hammer, "Raman Spectroscopic and Computational Analysis of the Effects of Noncovalent Interactions on DMSO," Poster, 2014 Mississippi State EPSCoR Meeting, Starkville, MS April 2014.

Kristina A. Cuellar*, "The Hydrophobic Effect: A Molecular Perspective." Seminar, The University of Mississippi Department of Chemistry and Biochemistry, December 2013

Kristina A. Cuellar*, Katherine L. Munroe, David H. Magers, N.I. Hammer, "Investigations of Noncovalent Interactions in Micro-solvated Networks of Trimethylamine N-oxide." Poster, 2013 Mississippi EPSCoR State Meeting, Hattiesburg, MS April 2013

Loan Tran*, **Kristina A. Cuellar**, John T. Kelley, Gregory S. Tschumper, N.I. Hammer, "Effects of Microsolvation on Pyrazine, Pyridazine, and S-triazine." Poster, 2013 Mississippi EPSCoR State Meeting, Hattiesburg, MS April 2013

Kristina A. Cuellar*, Katherine L. Munroe, David H. Magers, N.I. Hammer, "Investigations of Noncovalent Interactions in Micro-solvated Networks of Trimethylamine N-oxide." Poster, 2013 ACS National Meeting, New Orleans, LA April 2013

Loan Tran*, **Kristina A. Cuellar**, John T. Kelley, Gregory S. Tschumper, N.I. Hammer, "Effects of Microsolvation on Pyrazine, Pyridazine, and S-triazine." Poster, 2013 ACS National Meeting, New Orleans, LA April 2013

Kristina A. Cuellar*, Katherine L. Munroe, David H. Magers, N.I. Hammer, "Investigations of Noncovalent Interactions in Micro-solvated Networks of Trimethylamine N-oxide." Poster, 2012 Mississippi EPSCoR State Meeting, University, MS April 2012

Joseph Golden***, Kristina Cuellar**, Charles L. Hussey, Gregory S. Tschumper, and Nathan I. Hammer, "Effects of Micro-Solvation on Room Temperature Ionic Liquids" Poster, 2012 Mississippi EPSCoR State Meeting, University, MS April 2012

Kristina A. Cuellar*, Katherine L. Munroe, David H. Magers, N.I. Hammer, "Investigations of Noncovalent Interactions in Micro-solvated Networks of Trimethylamine N-oxide." 32nd Undergraduate Research Conference at the University of Memphis, Memphis, TN February 2012

Katherine L. Munroe***,** David H. Magers, **Kristina A. Cuellar**, N. I. Hammer, "Investigations of Noncovalent Interactions in Micro-solvated Networks of Trimethylamine N-oxide." 2011 Conference on Current Trends in Computational Chemistry, Jackson State University, MS, October 2011.

Outreach Activities

Affiliation: The University of Mississippi, Department of Chemistry and Biochemistry

Chemistry Demonstration – "Liquid Nitrogen Ice Cream to Dippin' Dots," Lafayette Middle School, Ms. Foster's 7th Grade Science Class (22 students), April 23, 2013, participant with Professor T. Keith Hollis and Ginger Tyson. Taught Cold vs. lack of Heat with dry ice (sublimation demo) and liquid nitrogen.

Chemistry Demonstration – "Liquid Nitrogen Ice Cream to Dippin' Dots," Lafayette High School, Ms. Wamble's Chemistry and Physical Science classes (37 students), April 23, 2013, participant with Professor T. Keith Hollis and Ginger Tyson. Taught Cold vs. lack of Heat with dry ice (sublimation demo) and liquid nitrogen.

Chemistry Demonstration – "Liquid Nitrogen Ice Cream to Dippin' Dots," Mississippi NSF EPSCoR Science Teacher Training (13 MS Middle School and 1 High School Science Teachers), June 10, 2013, participant with Professor T. Keith Hollis and Ginger Tyson. Taught Cold vs. lack of Heat with dry ice (sublimation demo) and liquid nitrogen.